

Provided for non-commercial research and education use.  
Not for reproduction, distribution or commercial use.



This article appeared in a journal published by Elsevier. The attached copy is furnished to the author for internal non-commercial research and education use, including for instruction at the authors institution and sharing with colleagues.

Other uses, including reproduction and distribution, or selling or licensing copies, or posting to personal, institutional or third party websites are prohibited.

In most cases authors are permitted to post their version of the article (e.g. in Word or Tex form) to their personal website or institutional repository. Authors requiring further information regarding Elsevier's archiving and manuscript policies are encouraged to visit:

<http://www.elsevier.com/copyright>



## Research paper

## Osmotic properties of auditory hair cells in the leopard frog: Evidence for water-permeable channels

Nasser A. Farahbakhsh<sup>a,\*</sup>, Jaime E. Zelaya<sup>a</sup>, Peter M. Narins<sup>a,b</sup><sup>a</sup> Department of Integrative Biology and Physiology, 621 Charles E. Young Drive S, University of California, Los Angeles, CA 90095 1606, USA<sup>b</sup> Department of Ecology & Evolutionary Biology, 621 Charles E. Young Drive S, University of California, Los Angeles, CA 90095 1606, USA

## ARTICLE INFO

## Article history:

Received 13 August 2010

Received in revised form

1 October 2010

Accepted 26 October 2010

Available online 31 October 2010

## ABSTRACT

When amphibian papillar hair cells (APHCs) of the leopard frog, *Rana pipiens pipiens*, are osmotically challenged, they exhibit a characteristically asymmetric (rectifying) response: small decreases (5%, or less) in the extracellular solution's osmolarity do not significantly affect the cells' volume; larger decreases produce a relatively slow volume increase in APHCs, while exposure to a hyperosmotic medium leads to rapid shrinking of these cells. Furthermore, the rate of volume change appears to be a function of the rate of extracellular osmotic change.

These characteristics make the application of methods devised for the estimation of the osmotic permeability coefficient ( $P_f$ ) for semipermeable membranes – i.e., those with significant permeability *only* to water – to APHC membrane rather futile. We have, therefore, devised a method that takes both the permeability to solutes as well as the kinetics of the osmolarity change into consideration, in order to obtain estimates of  $P_f$  that are to a large degree independent of these factors. We have compared the new and earlier methods.

Using the new method, we have estimated the  $P_f$  of APHCs' plasma membrane to be in the  $10^{-2}$ -cm/s range, and thus significantly larger than those reported for lipid bilayers. APHC's membrane  $P_f$  appears to be cell-size independent and insensitive to extracellular mercury. These results suggest that APHCs express water-permeable channels in their plasma membrane. Furthermore, we suggest that asymmetric and rate dependent shape changes produced by osmolarity changes in APHCs imply the presence of significant permeability to solutes. The significance of transmembrane solute transport and water channel expression in amphibian auditory hair cells is discussed.

© 2010 Elsevier B.V. All rights reserved.

## 1. Introduction

Auditory hair cells of the leopard frog, *Rana pipiens pipiens*, exhibit a significantly larger permeability to water than their mammalian counterparts. The presence of a readily-available ('immediate') volume regulatory mechanism in these cells, however, undermines the utility in this preparation of methods originally developed for estimation of the osmotic permeability coefficient for semipermeable membranes (i.e., those with negligible permeability to ions and molecules other than water). Here we show that minimizing the effects of osmotically-induced solute transport across the membrane (and therefore, volume regulation)

by measuring the small volume change induced at the onset of each osmotic challenge, while estimating the transmembrane osmotic difference from the time course of solution change in the cell's vicinity, will produce reasonable estimates of the osmotic permeability coefficient. It should be emphasized, however, our main goal in this manuscript is measuring the osmotic permeability coefficient of APHCs' membrane, and not identifying the solute(s) transported across the cell membrane or transporting mechanisms involved. These latter aims are beyond the scope of this work.

In two recent reports (Farahbakhsh and Narins, 2006, 2008), we described a calcium-dependent mechanism that can potentially mediate the process of slow motility in low-frequency auditory hair cells of amphibians. Furthermore, we developed a method for quantitative analysis of shape change in isolated hair cells and devised a model for identifying different aspects of the response to agents that modulate the geometrical attributes of these cells. This method allowed us to identify three distinct but temporally overlapping periods in the shape change induced by the calcium ionophore, ionomycin, in hair cells dissociated from the rostral

Abbreviations: AP, amphibian papilla; APHC, AP hair cell;  $[Ca^{2+}]_i$ , intracellular free calcium concentration; DIC, differential interference contrast; IHC, inner hair cells; OHC, outer hair cells; RVD, regulatory volume decrease; RVI, regulatory volume increase.

\* Corresponding author. Tel.: +1 310 206 4343.

E-mail address: [farahbak@ucla.edu](mailto:farahbak@ucla.edu) (N.A. Farahbakhsh).

region of the amphibian papilla (RAPHCs), one of the two auditory organs in frogs. During phase 1 of the response to ionomycin, these hair cells undergo a brief ( $\approx 50$  s long) and slow ( $\approx 300$  nm/s) contraction-like isovolumetric shortening. This episode is then followed by a somewhat longer ( $\approx 90$  s) period during which continued length decrease is accompanied by an increase in the cells' volume (phase 2, or "osmotic" shortening), which has also been observed in OHCs (Dulon and Schacht, 1992). In the last stage of the response (phase 3), the cells' length and volume increase together.

In those earlier experiments our attention was mostly focused on the mechanism of isovolumetric shortening in RAPHCs. However, we also quantified these cells' ability to change their volume in an iso-osmotic medium, which suggested the presence of mechanisms for transporting solutes across the cell membrane, as well as a significant permeability to water. In the experiments reported here we have attempted to measure the osmotic permeability coefficient of auditory hair cells in the amphibian papilla (APHCs) of the leopard frog, and to further our understanding of transport mechanisms in amphibian hair cells. Our findings suggest that (a) the APHC membrane has an osmotic permeability coefficient ( $P_f$ ) significantly larger than that of a lipid bilayer, and (b) when exposed to a hypo-osmotic challenge, APHCs exhibit an immediate volume regulatory response, possibly through the release of a significant amount of existing intracellular solutes through readily utilizable pathways. This response is distinct from the classical regulatory volume decrease (RVD) triggered by an initial change in the cell volume, which in APHCs appears with a delay of more than 5 min.

As we report here, a cytoplasmic membrane with considerable permeability to both water and solutes provides an APHC with the ability to regulate its volume and maintain its shape, and thus preserve the level of its vitally-important mechanical, electrical and chemical activities, despite changes in the extracellular osmolarity. A summary of these results was presented at the 33rd meeting of the Association for Research in Otolaryngology (Farahbakhsh et al., 2010).

## 2. Methods

### 2.1. Dissociation of hair cells

Amphibian papillae (APs) were dissected out of pithed and decapitated adult northern leopard frogs (*R. pipiens pipiens*), and hair cells were gently scraped free from trypsin-treated APs in the recording chamber as described previously (Farahbakhsh and Narins, 2006). The recording chamber was then placed on the stage of an inverted microscope (Zeiss Axio Observer Z1, Germany), and the hair cells within the microscope viewfield were continuously imaged with a  $100\times/1.3$  oil immersion plan-neofluar objective (Zeiss) and components of differential interference contrast (DIC) and/or fluorescence microscopy, as needed. The microscope was equipped with hardware and software modules required for real-time image acquisition, analysis and storage (SlideBook, Intelligent Imaging Innovations, Inc. Denver, CO).

AP hair cells were bathed in or perfused with a perilymph-like standard external solution (Bernard et al., 1986), herein referred to as the AP solution. The AP solution contained (in mM): NaCl, 110; KCl, 2; CaCl<sub>2</sub>, 2; MgCl<sub>2</sub>, 0.8; D-glucose, 3; HEPES, 10. pH was adjusted to 7.2, with NaOH. Osmolarity was adjusted to 223–227 mosmol l<sup>-1</sup> with a vapor pressure osmometer (Vescor, model 5520, Logan, UT). In order to make hypoosmotic solutions, appropriate amount of double-distilled water was added to the AP solution. For hyperosmotic solutions, the AP solution was supplemented with appropriate amounts of sucrose. In some experiments, concentrated sucrose solutions were directly injected into the chamber filled with the AP solution (see below).

### 2.2. The chamber and experimental setup

The recording chamber consisted of a 35-mm plastic petri dish, specially modified by cutting a hole about 14 mm in diameter into its bottom and cementing a 25-mm microscope glass cover slip under the hole with paraffin. A plastic insert was placed in the petri dish to reduce the effective volume of the chamber to 500  $\mu$ l, to provide an input and output for the perfusion system (Fig. 1A), and to hold the thermometer probe. In experiments in which hair cells were continuously perfused, the complete time course of shape change was obtained by recording the DIC and/or fluorescence image of the hair cells for a 20-min-period in which the first 5 min, cells were perfused with the AP solution, then perfusate was changed to either hypo- or hyperosmotic solutions for the next 5 min, and finally, the chamber was washed out by perfusing with the AP solution for additional 10 min to allow for the recovery of cell shape. To investigate the effect of inhibitors, the osmotic challenge was preceded by 5 min of pretreatment of APHCs with the inhibitor, which was also included in the perfusate throughout the osmotic challenge.

Dissociated AP hair cells can readily but partially (usually only in one spot) adhere and remain attached to the glass substrate without any need for adhesive compounds. In the majority of recordings, this partial attachment did not impede cell's ability to change its shape. Data from experiments in which cell appeared flattened, or adhesion to the substrate limited the shape change, were excluded. In experiments in which solution change was carried out by bath perfusion, the rate of solution flow in the chamber was kept constant throughout the recording at 1.6 ml/min, which was determined to be the maximum flow rate possible without significant perturbation and dislodgement of the cells. At this flow rate, the bulk solution in the recording chamber is expected to be replaced more than three times per minute. However, the rate of solution change in the vicinity of attached hair cells was found to be significantly lower. The fluorescent dye 2',7'-dichlorofluorescein (Sigma) was used to determine the rate of solution change in a 50  $\mu$ m by 28  $\mu$ m area in the center of the chamber. Both the time constant of fluorescence increase in the imaged area, upon introduction of the dye into the chamber, as well as the time constant of fluorescence decrease during the washout were found to depend on the concentration of dichlorofluorescein used: the higher the dye concentration the faster the fluorescence increase and slower the decline. This nonlinear dose–response relationship results from the overlap of excitation and emission spectra of fluorescein – a phenomenon known as "self-quenching" (Lakowicz, 1983).

Very low concentrations of fluorescein, however, produced a very poor signal-to-noise ratio, which made time constant estimates unreliable. We found the range of 62.5–250  $\mu$ g/ml AP solution to be the optimum concentration range for this dye. As shown in Fig. 1B, the time course of fluorescence increase (mean  $\pm$  SEM of six measurements) for the AP solution containing 125  $\mu$ g/ml 2',7'-dichlorofluorescein and 0.5% ethanol, could be satisfactorily fitted with a single exponential with the time constant,  $\tau = 47.5$  s. The mean and standard deviation of the time constant of exponential curves fitted to individual fluorescence time courses were,  $\tau = 49.0 \pm 2.2$  s. In the same measurements, the time constant of fluorescence decrease during the washout period was  $\tau = 90.2 \pm 3.3$  s. In estimating hair cells' osmotic permeability coefficient, we have assumed the time constant of solution change in the vicinity of hair cells to be,  $\tau = 47.5$  s, except when the time constant of cell's volume change was found to be smaller than 47.5 s. In such cases (9 in 85 measurements; see Fig. 3B), the time constant of solution change was assumed to be the same as that of the volume change (e.g., the volume decrease phase in the lower panel of Fig. 3A).

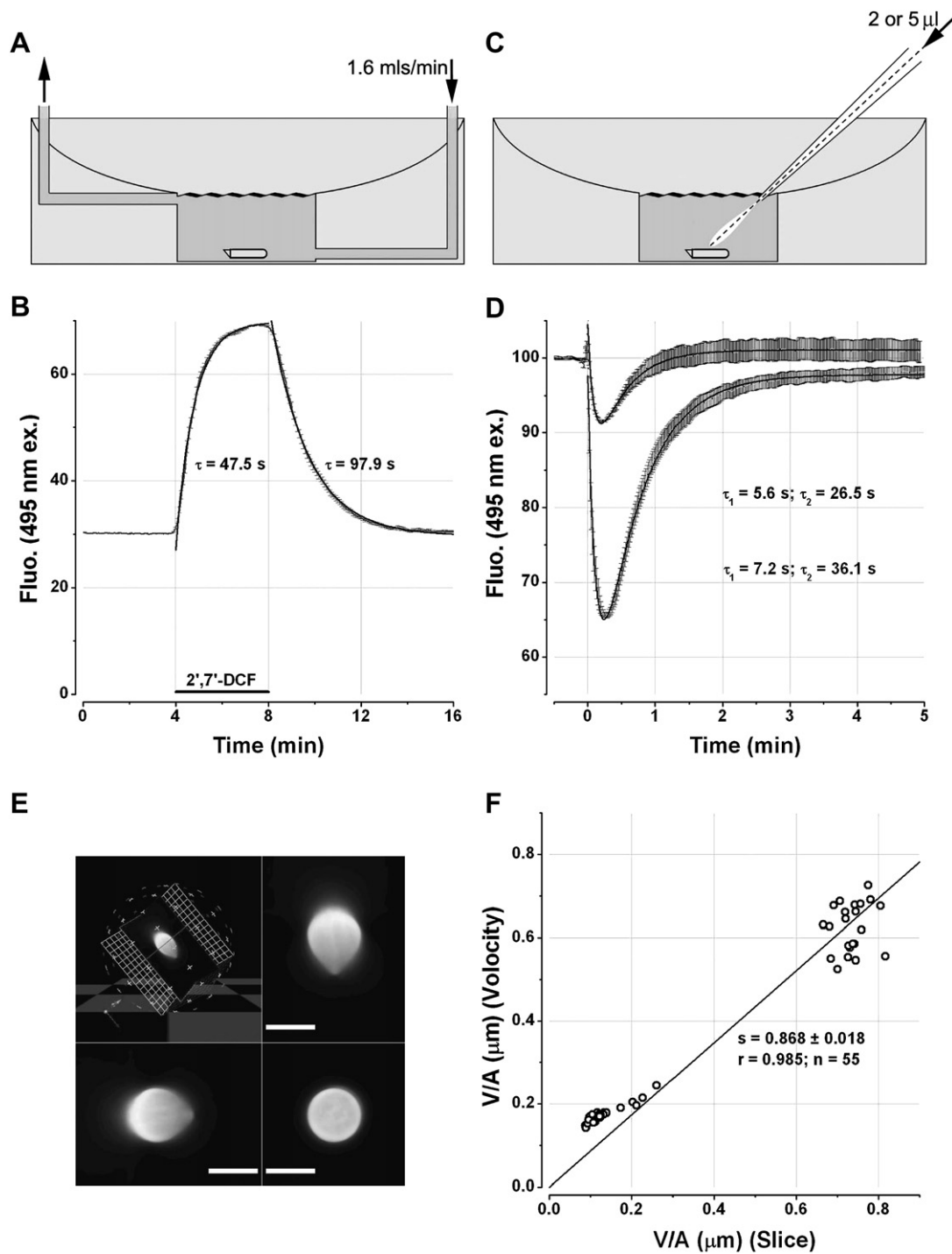


**Fig. 1.** Experimental setup. A: cross-section of the recording chamber showing the position of the perfusion system's inflow and outflow tubes. B: the time course of fluorescence intensity change (grey) as 125  $\mu\text{g/ml}$  2',7'-dichlorofluorescein was perfused through the chamber for 4 min as indicated by the bar. Single-exponential curves (black) fitted to the rising and falling phases of the fluorescence intensity had time constants 47.5 and 97.9 s, respectively. C: cross-section of the chamber and pipette used for the injection experiments. The latter had a tip diameter of 0.38 mm, and was placed about 5 mm from the bottom center of the chamber. D: the time course of fluorescence change when either 2 or 5  $\mu\text{l}$  of 1.5 M sucrose solution is injected into the chamber filled with 250  $\mu\text{g/ml}$  2',7'-dichlorofluorescein. The mean and SEM of six measurements for 2  $\mu\text{l}$  (dark grey), and nine measurements for 5  $\mu\text{l}$  (light grey) injected sucrose are shown. Also shown are the sum of two exponentials (black) fitted to each time course. The time constants given are for the 2  $\mu\text{l}$  (5.6 and 26.5 s), and 5  $\mu\text{l}$  injections (7.2 and 36.1 s). E: three-dimensional confocal microscope image of a fluorescent spherical bead (nominal diameter, 4.2  $\mu\text{m}$ ) displayed in three perpendicular central cross-sections, and a tilted perspective, clearly displaying the distortion of objects along the z-axis. Scale bars: 4  $\mu\text{m}$ . F: comparison of the volume/area (V/A) ratio of 55 fluorescent spherical beads imaged by confocal microscope, estimated by a commercial program (Volocity) and our custom-made software (Slice). The slope of the line fitted to data points by linear least-squares regression show a 13% difference between the two estimates of V/A-ratio.

### 2.3. Osmotic challenge by injection

The injection device was composed of a tapered pipette with a 0.38-mm diameter orifice through which a fixed volume (2 or

5  $\mu\text{l}$ ) of concentrated sucrose (250 mM–1.5 M) was injected in 100 ms. In order to achieve a rapid and uniform exchange of solution surrounding APHCs, the tip of the pipette was immersed in the chamber solution, positioned about 5 mm from, and pointed

toward the center of the hair cells within the microscope viewfield (Fig. 1C). The perfusion pump was stopped, before the injection was initiated, to minimize the mixing and washout effects of the perfusate.

To characterize the kinetics of the injection setup, the recording chamber was filled with AP solution containing 250  $\mu\text{g/ml}$  2',7'-dichlorofluorescein and 10% ethanol. Either 2 or 5  $\mu\text{l}$  of 1.5-M sucrose was injected into the chamber while the fluorescence intensity of the dye within the 50  $\mu\text{m}$  by 28  $\mu\text{m}$  imaging area was measured. The injection produced a biphasic change in the recorded fluorescence intensity that could be fitted with the sum of two exponential functions. In six measurements for the injection of 2  $\mu\text{l}$  sucrose, the time constants for exponential curves were  $\tau_1 = 5.9 \pm 0.8$  s, and  $\tau_2 = 27.1 \pm 2.2$  s. Fig. 1D shows the average curve (and the standard error at each time point) for these six measurements. The fitted exponentials to the average curve have the time constants of 5.6 and 26.5 s. In nine similar measurements for the injection of 5  $\mu\text{l}$  of 1.5 M sucrose, the fitted bi-exponential curves had the time constants,  $\tau_1 = 7.1 \pm 0.7$  s, and  $\tau_2 = 34.9 \pm 2.4$  s. The average curve for these nine measurements was fitted with two exponentials with time constants, 7.2 and 36.1 s (Fig. 1D). These measurements indicate that our injection setup was able to exchange the solution surrounding hair cells with kinetics six to eight times faster than our perfusion system.

#### 2.4. Hair cell length and volume measurements

The rate of image acquisition was varied throughout each experiment in order to accommodate the need for recording events with varying speed, while minimizing the number of images to be analyzed. In general, in each experiment the rate was changed from one image series (DIC and fluorescence) per second to one every 30 s. For the off-line data analysis, two different but comparable methods were used. In the majority of experiments reported here, individual DIC images were digitized and displayed on the computer screen, and the contour of the hair cell soma was traced manually. When faster analysis of large number of images was needed, cells were loaded with the fluorescent dyes calcein (Molecular Probe, Eugene, OR), and excited at 488 nm. The contour of hair cells in the acquired fluorescence images were then determined by an adaptive-threshold method (similar to features available in the commercial program, Volocity, Perkin Elmer) that corrected for changes in the fluorescence level caused by the volume change, dye bleach and leakage, and other experimental artifacts that affect fluorescence intensity.

In either case, the contour line was then analyzed using custom-made software (Slice) to determine the cell's length and cross-sectional area. The cell's average diameter and volume were then estimated as described previously (Farahbakhsh and Narins, 2006). Briefly, the average cell diameter is taken as the ratio of the cross-sectional area and length, and the volume is estimated by slicing the cell's image perpendicular to its longer axis. The thickness of each slice is not larger than one pixel size (0.129  $\mu\text{m}$ ). Then, the volume of each slice is calculated by assuming it is a circular cylinder with a diameter equal to the cell's width in that slice (Farahbakhsh and Narins, 2006).

For cells exposed to mercury showing blebbing, the volume of cell soma was estimated as above. Blebs were assumed to be either a sphere or a spherical cap, as judged by eye. The volume of a spherical bleb was estimated by measuring its diameter; and for a spherical cap, its base diameter and height.

In order to validate our method of volume estimation we used a confocal microscope (model TCS SP, Leica) to reconstruct the 3-D structure of a number of APHCs, as well as that of fluorescent spherical beads (FluoSpheres, Invitrogen, Carlsbad, CA). Our

measurements indicate that confocal microscope distorted these images (see Fig. 1E), causing a 20% overestimation in the calculated volume, which appeared to be independent of the bead or cell size (Farahbakhsh and Narins, 2008). However, because of an even larger overestimation of the surface area by the confocal microscope, the ratio of volume/surface area ( $V/A$ ) estimated by the 3-D reconstruction software (Volocity) is about 13% smaller than that calculated on the basis of our cell model (Fig. 1F). Since the osmotic permeability coefficient,  $P_f$ , of cells depends only on their  $V/A$  ratio, and not any other geometrical parameter (see below), these calibration measurements indicate that our estimates of  $P_f$  are at most 15% larger than those we would have made had we performed all our experiments under a confocal microscope.

#### 2.5. Data analysis

Changes in the measured length and cross-sectional area, as well as estimated average diameter and somatic volume were calculated and compared between different episodes in each experiment (baseline condition, osmotic challenge, and recovery during the washout period), and between similar experiments. The relationship between the APHC volume and the extracellular osmolarity was fitted to the normalized version of the Boyle–Van't Hoff equation for an ideal osmometer (Probstein, 1994),

$$V = k/C + V_{\text{solid}} \quad (1)$$

where  $V$  is the cell volume;  $C$ , extracellular osmolarity;  $V_{\text{solid}}$ , volume of the osmotically-inactive part of the cell; and  $k$ , a constant. The normalized version of this equation is written as,

$$V/V_0 = \phi/(C/C_0) + 1 - \phi \quad (2)$$

where  $V_0$  and  $C_0$  are the initial cell volume and osmolarity, respectively; and  $\phi = k/V_0C_0$ . For an ideal osmometer,  $0 < \phi \leq 1$ .

In addition we used these osmotically-induced volume changes to calculate the osmotic permeability coefficient ( $P_f$ ) of APHCs. To that end, we utilized three different approaches. In the first, we inserted the parameters of the least-squares fit of a single-exponential curve,  $a(1 - e^{-bt})$  to the normalized osmotically-induced volume change, into the linear relationship,

$$50abr_0/V_W = P_f\Delta C \quad (3)$$

where  $r_0$  is the APHC's initial average (estimated) radius;  $V_W$ , the partial molal volume of water (18  $\text{cm}^3/\text{mole}$ ); and  $\Delta C$ , the imposed osmotic difference (Ratnanather et al., 1996; Zhi et al., 2007). An estimate of  $P_f$  was made as the slope of the fitted line to the data pooled from a large number of similar experiments (e.g., in Fig. 3C).

In the second approach, the pooled data were fitted to the linear relationship,

$$(\kappa\tau)^{-1} = P_f\pi^2 \quad (4)$$

where  $\kappa = V_W C_0 A / \phi V_0$ ;  $A$  is the APHC's plasma membrane area;  $\phi$ , the osmotically active fraction of the cell volume at the start of the osmotic challenge;  $\tau$ , the time constant of the exponential function fitted to the volume change ( $=1/b$ ); and  $\pi$  is the relative extracellular osmolarity [ $=C(\infty)/C(0)$ ] (Farmer and Macey, 1970). For the experiments reported here, we estimated the APHCs' membrane area as  $A = 2\pi r_0 l + 2\pi r_0^2$ , where  $l$  is the cell's length.

These approaches yield reliable estimates of  $P_f$  only if (a), the cell membrane is semipermeable, i.e., permeable only to water, and not to any solute; and (b), the rate of osmolarity change is much higher than that of the volume change. APHCs appear to have significant permeability for solute(s); and are also capable of changing their volumes almost as fast as the osmotic changes employed in our

experiments. As a result, fitting the APHCs' data to the equation (3) or (4) is expected to produce underestimates of the osmotic permeability coefficient in APHCs (see Results). To minimize the adverse effects of solute permeability and slow perfusion, we used a 'small-signal' approach to estimate the APHCs'  $P_f$ . According to the Van't Hoff's law,

$$J_v = P_f V_w A \Delta C \quad (5)$$

where  $J_v$  is the volume flow of water. In a closed cell,  $J_v = dV(t)/dt$ , where  $V(t)$  is the cell's volume at time,  $t$ . Thus, equation (5) can be written as,

$$P_f = (dV(t)/dt)/V_w A \Delta C(t) \quad (6)$$

$dV(t)/dt$  and  $\Delta C(t)$  were calculated for each time point during the time course of the response to an osmotic challenge. For both perfusion and injection experiments,  $\Delta C(t)$  was estimated for each time point from the kinetics of fluorescence change in the extracellular medium, during the onset of solution change, as described above (Fig. 1B and D). The maximum value of  $(dV(t)/dt)/V_w A \Delta C(t)$  was selected as the APHC's  $P_f$  (Belyantseva et al., 2000). Because of the (approximately) single-exponential character of both osmolarity and volume changes, the data collected at the first sample point after the start of volume change ( $t=5$  s, for the perfusion experiments; and  $t=1$  s, for the injection experiments) always yielded the largest estimate for  $P_f$ . It is noteworthy that in this approach, the estimated  $P_f$  is susceptible to the error in calculation of the derivative of the volume. The (approximately) exponential character of the volume change time course, however, allows one to substitute  $dV(t)/dt$  in the equation (6) with,

$$dV(t)/dt = [(V_\infty - V_0)/\tau]e^{-t/\tau} \quad (7)$$

where,  $V_\infty$  is the steady-state volume produced by the osmotic challenge.

Statistical significance was determined using the one-way ANOVA or paired two-sample  $t$ -test, wherever applicable.  $p < 0.05$  was considered statistically significant.

## 2.6. Chemicals

Calcein-acetoxymethyl (AM) ester and ionomycin were obtained from Molecular Probes (Eugene, OR). Other chemicals were purchased from Sigma (Milwaukee, WI). Calcein-AM and ionomycin were dissolved in DMSO, and the stock solutions were kept at  $-20^\circ\text{C}$ . At the time of the experiment, these stocks were diluted into the AP solution. The final concentration of DMSO in the AP solution was kept at 0.1%, or less.

## 2.7. Animal care

The care and use of animals reported in this study were approved by the University of California at Los Angeles Chancellor's Animal Research Committee (ARC number 1994-086-52).

## 3. Results

### 3.1. Osmotic challenge by perfusion

Hair cells dissociated from the amphibian papilla (APHCs) maintain their geometrical shape for more than an hour when continuously perfused with a perilymph-like solution (AP solution; osmolarity, 223–227 mosmol $^{-1}$ ; for composition, see Methods). They are also quite resilient when osmotically challenged: they can tolerate and largely rebound from exposure to a 50% osmotic

change in either direction. In the experiment shown in Fig. 2A, a 53- $\mu\text{m}$ -long APHC was perfused with the AP solution for 5 min during which it showed no significant change in any of its physical parameters (e.g., length, cross-sectional area, or calculated volume). A 5-min perfusion with a 50% hypoosmotic solution, however, produced an 8.2% decrease in cell length and a 64.6% increase in cell volume. Had this cell had a semipermeable cytoplasmic membrane ('an ideal osmometer'), the osmotically active fraction of its original volume could have been estimated from equation (2),  $\phi = 0.646$ . Upon return to the iso-osmotic AP solution, this hair cell regained its original length (within 0.6%). However, at the end of the 10-min recovery period, its volume had dropped to 91.7% of the initial value. In other words, increasing the osmolarity of the perfusate from 50% to 100% (during the recovery) caused a volume decrease of 44.3%. For an ideal osmometer, this ratio indicates that 88.6% of the cell volume at the start of recovery, or a fraction  $\phi = 0.812$  of the cell's initial volume was osmotically active during this phase. The difference between these two estimates of  $\phi$  ( $0.812 - 0.646 = 0.166$ ), suggests that at least one-sixth of the cell's initial osmolytes were released during the 5-min exposure to the 50% solution. A video clip showing the time course of this experiment is included in the Supplement.

Supplementary video related to this article can be found at doi: 10.1016/j.heares.2010.10.015

In five similar experiments, the APHC volume increased by  $48.3 \pm 7.8\%$  in response to the 50% hypoosmotic challenge (Fig. 2E). Interestingly, in the 5-min long exposure to the hypoosmotic solution none of these cells exhibited a biphasic volume change commonly associated with the phenomenon of regulatory volume decrease (RVD) (Hoffmann et al., 2009) during this period (see Discussion). By the end of the 10-min washout period, however, the volume fell to  $92.2 \pm 2.5\%$  of its initial level. For this group of APHCs, volume decrease during the recovery was  $37.3 \pm 3.5\%$ . Thus, the minimum amount of intracellular osmolytes released during the period of exposure to the 50% solution was estimated to be  $15.7 \pm 5.0\%$  of the initial amount. Qualitatively similar results were recorded in response to the 75% hypoosmotic challenge (not shown). APHCs' volume was increased by  $14.6 \pm 2.5\%$  in response to 25% decrease in the osmolarity. By the end of the 10-min recovery period, volume had dropped to  $96.8 \pm 0.6\%$  of its initial value, or  $84.6 \pm 1.4\%$  of that at the start of the recovery period. The osmolytes released by the cells in this group of experiments amounted to no less than  $12.9 \pm 2.3\%$  of the initial amount.

Somewhat different responses were recorded for smaller hypoosmotic challenges. Fig. 2B shows the mean  $\pm$  SEM of responses of four APHCs to the 95% hypoosmotic solution. During the 5-min challenge, the cells' volume was increased by a statistically insignificant  $0.48 \pm 0.51\%$ . The cells' length also remained statistically unchanged ( $99.9 \pm 0.5\%$ ). However, upon return to the iso-osmotic AP solution, their volume decreased by  $4.8 \pm 1.1\%$  before displaying regulatory volume increase (RVI), as a result of which volume returned to within  $3.0 \pm 0.3\%$  of the baseline level, by the end of the 10-min wash. The absence of a measurable volume change in response to the 95% solution suggests that during the 5-min long period of exposure to this solution these APHCs should have released an equivalent of 5% of their osmotically active solutes in order to lower their intracellular osmolarity to the extracellular level. It should be noted that the method we used to estimate the fraction of solutes released by the 50% and 75% solutions would no longer have any utility for small hypoosmotic challenges that fail to induce a measurable volume change (e.g., the 95%), or when because of the small size of the volume change there is considerable variation in the result (e.g., the 90%). For the 90% solution this method produced quite variable estimates of the solute released ( $18.3 \pm 21.3\%$ ).

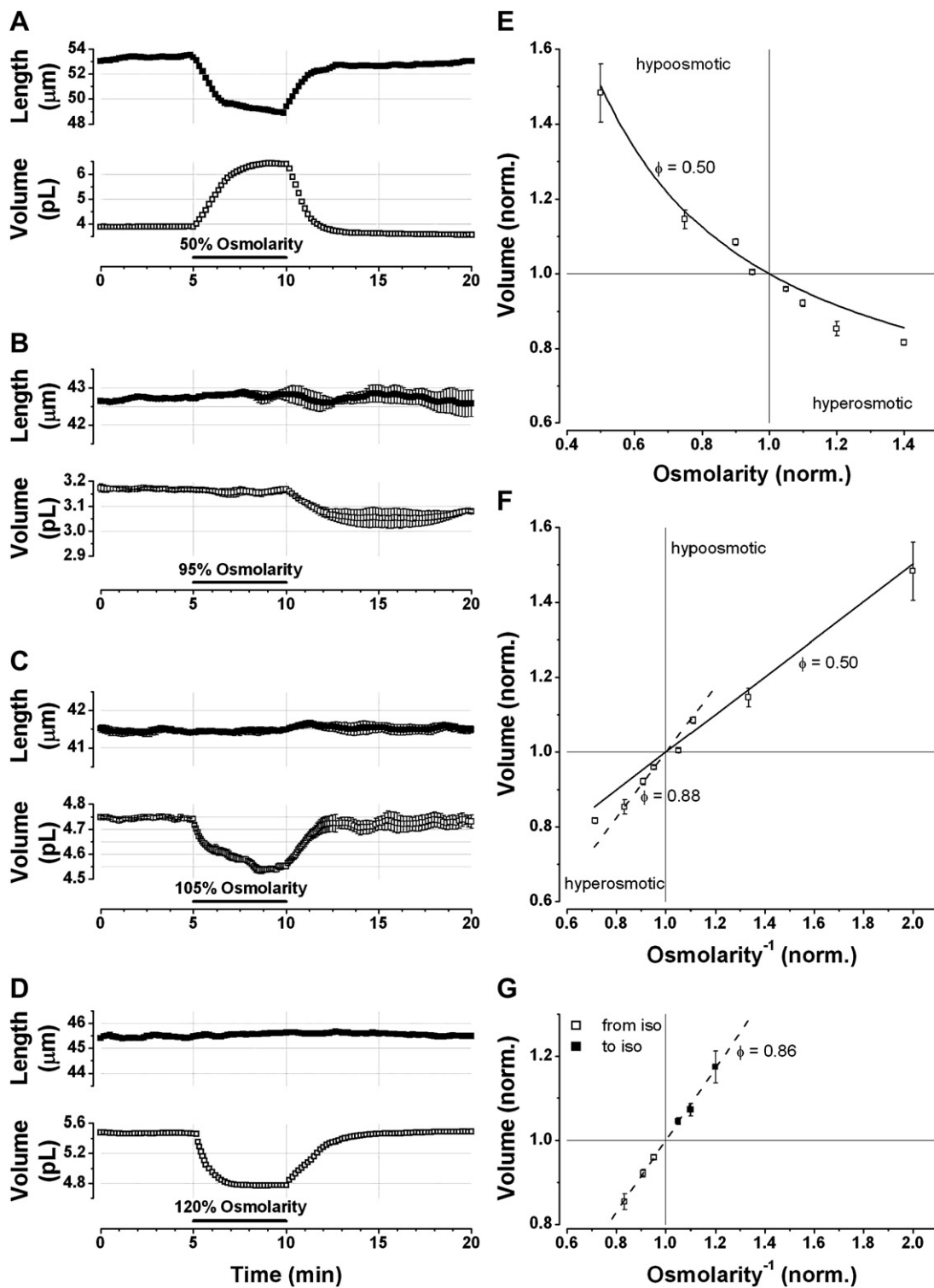


**Fig. 2.** Osmotically-induced shape change. **A:** the complete time course of length and volume changes for an APHC exposed to a 50% hypoosmotic solution for the period shown by the bar. Changes in APHC length (in  $\mu\text{m}$ ) and estimated volume (in picoliters =  $10^3 \mu\text{m}^3$ ) before, during and after exposure to the hypoosmotic solution are shown. **B:** time courses of the mean  $\pm$  SEM of length and volume of four APHCs exposed to 95% hypoosmotic solution. The bar shows the period of exposure to the hypoosmotic solution. The length and volume of all four cells were adjusted to have the same initial (at  $t=0$ ) values, which corresponded to the average of the four initial lengths and volumes, respectively. **C:** the responses of four APHCs to 105% osmotic solution. The time courses of mean  $\pm$  SEM of adjusted lengths and volumes are shown, as in Fig. 2B. **D:** the typical response of an APHC to a 120% osmotic solution. Note the different ordinate scale for the time course of volume compared to those of Fig. 2B and C. **E:** the relationship between volume and osmolarity, both normalized with respect to their values in the iso-osmotic (AP) solution. Each data point (open square and vertical lines) represents the mean  $\pm$  SEM of 5–7 measurements. The curve fitted to these data points represents the normalized Boyle–Van’t Hoff law (equation (2)), with  $\phi = 0.50$ . **F:** the relationship between volume and the inverse of osmolarity for the data shown in Fig. 2E. The solid line is the least square fit to all data points (slope,  $\phi = 0.50$ ), while the dashed line is the linear fit to the data points for 105–120% osmolarity (slope,  $\phi = 0.88$ ). **G:** the volume vs. inverse osmolarity for data points representing the response to 105–120% osmolarity (open squares), and for the recovery from the same osmotic challenges (closed squares). Slope of the dashed line fitted to these data points:  $\phi = 0.86$ .

APHCs exposed to small hyperosmotic challenges exhibited rapid and measurable shrinking. Fig. 2C depicts the mean  $\pm$  SEM response of four APHCs exposed for 5 min to the AP solution containing 11.25 mM added sucrose (the 105% solution). During this period, the cells' volume dropped to  $95.9 \pm 0.5\%$  of its baseline level. The response was readily reversible. During the following washout period in the iso-osmotic AP solution, the cells' volume recovered to  $100.5 \pm 0.6\%$  of the initial value.

In response to larger hyperosmotic shocks, APHCs showed a relatively fast volume decrease with little or no change in the length. In the experiment shown in Fig. 2D, perfusion with a 120% hyperosmotic solution (45 mM added sucrose) decreased the cell's volume by 12.7% in 5 min, while the length increased by less than 0.3%. In five similar experiments, cells shrank by  $14.7 \pm 1.9\%$  by the 120% hyperosmotic solution, while their length was left unchanged ( $99.9 \pm 0.5\%$ ). After return to the iso-osmotic AP solution, the cell in

Fig. 2D fully recovered its original volume (100.4% of the baseline volume by the end of 10 min washout). In the five cells in this group, 10 min perfusion with the AP solution returned the cells' volume to  $99.9 \pm 1.4\%$  of its baseline value. In three of five cells examined, the start of the recovery episode was delayed between 35 and 238 s (not shown). Qualitatively similar results were obtained when APHCs were perfused with 110% or 140% hyperosmotic solutions (not shown).

Fig. 2E summarizes the relative volume changes recorded in 46 experiments in which the response of APHCs to eight different osmolarity levels were recorded. For each osmolarity level, the mean and standard error of the final volume (normalized with respect to each APHC's initial volume,  $V_{\infty}/V_0$ ) are shown. The solid curve represents the least squares fit of these experimental data to the normalized version of the Boyle–Van't Hoff equation for an ideal osmometer (see equation (2)). Fig. 2F shows the relation

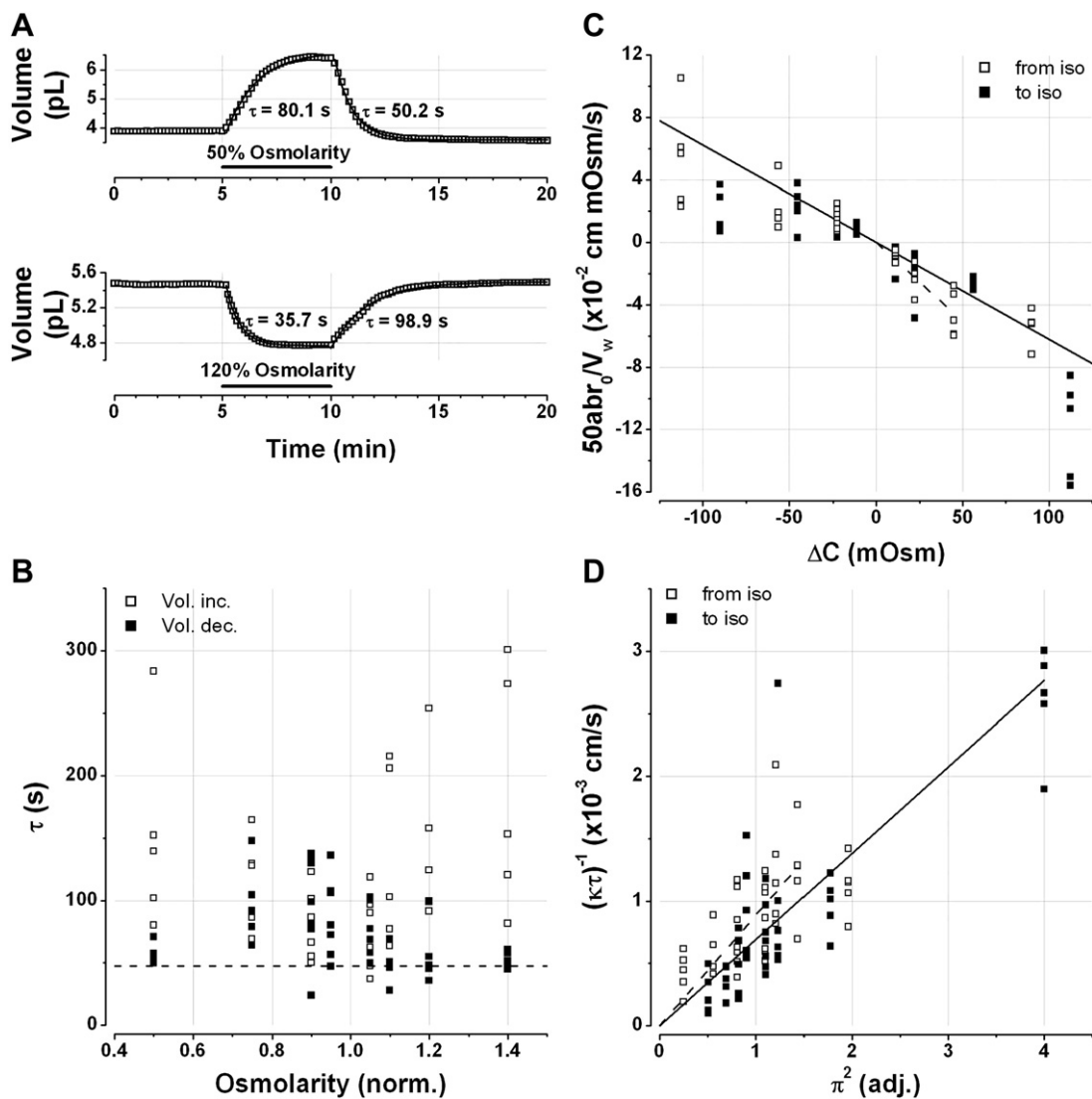


**Fig. 3.** Kinetics of osmotically-induced volume change. A: single-exponentials fitted to the response and recovery episodes of osmotically-induced volume change for the two APHCs shown in Fig. 2A and D (solid curves). The time constant for each exponential curve is also indicated. B: time constants (in s) of osmotically-induced volume increase (open squares) and decrease (closed squares) calculated from data collected in 46 experiments are shown as a function of the relative osmolarity. The dashed line represents the time constant of the perfusion system (47.5 s). C: a rearranged version of Fig. 3B, in which the inverse of each time constant ( $b = 1/\tau$ ) is weighted by the relative size of the response ( $a$ ) and by APHC's average radius ( $r_0$ ) and plotted against the osmotic change ( $\Delta C$ ). Data points for both the response starting in the iso-osmotic solution (open squares) and the recovery episode (closed squares) are included. The solid line fitted to all data points has a slope,  $s_{\text{all}} = -6.2 \pm 0.4 \times 10^{-4}$  cm/s. The dashed line fitted to data points corresponding to 17 volume decreases recorded in response to 105–120% osmolarity, has a slope,  $-10.1 \pm 0.8 \times 10^{-4}$  cm/s. D: presentation of the time constant vs. osmolarity relationship according to the model of Farmer and Macey (1970). The solid line fitted to all data points has a slope,  $s = 6.9 \pm 0.3 \times 10^{-4}$  cm/s. The dashed line is fitted to data obtained from the volume decreases in response to 105–120% osmolarity, and has a slope of  $8.9 \pm 0.8 \times 10^{-4}$  cm/s.

between the APHCs' volume and the inverse of osmolarity (both normalized). For an ideal osmometer, this latter relationship is linear, with the proviso that fitted line must pass through the point 1:1. However, the data presented in this figure suggest that APHCs exposed to osmotic challenge behave in ways far from an ideal osmometer, namely, (1) some data points (e.g., for 95% hypo-osmotic challenge) display a significant deviation from the Boyle–Van't Hoff equation, and (2) the responses to the hypoosmotic and hyperosmotic solutions are not symmetrical as expected from an ideal osmometer: while the least squares linear fit to all data points (or, to only the responses to 50%–95% osmolarity), has a slope of  $\phi = 0.5$ , the data points for 105% through 120% osmolarity can be fitted to a line with a slope of  $\phi = 0.88$  (the dashed line in Fig. 2F). Interestingly, the volume changes during the recovery phase of the response to 105–120% osmolarity challenges also fall on the same line as the one fitted to the points representing the osmotically-induced volume decreases (Fig. 2G). As described above, we attribute these deviations from osmometric behavior to APHCs' permeability to intracellular solutes.

### 3.2. Kinetics of osmotically-induced volume change

As reported previously for mammalian outer hair cells (OHCs; Ratnanather et al., 1996; Belyantseva et al., 2000; Zhi et al., 2007), the onset phase of the time course of an osmotically-induced volume change in APHCs could be approximated with a single exponential curve. Moreover, in APHCs, the time course of volume recovery upon return to the iso-osmotic solution also followed an approximately exponential trajectory. Fig. 3A depicts the single exponential curves fitted to the two examples shown in Fig. 2A and D. Fig. 3B displays the relationship between 85 time constants (in seconds) measured in 46 experiments, and the osmolarity of the applied challenge (normalized). Table 1 summarizes the mean and SEM of the time constants for each osmotic challenge.

As discussed by Ratnanather et al. (1996), a gradual change in the extracellular osmolarity, produced by bath–perfusion systems of the type utilized in our experiments, is expected to introduce a second exponential component in the volume–change time course that represents the kinetics of solution change. While fitting the volume–change trajectory with the sum of two exponentials consistently produced a “better” fit, it failed to generate two time constants clearly identifiable with the solution and volume changes.

This problem was particularly severe for the volume-decrease time courses: In some cases, the two time constants were almost identical, and in others too far apart, to be realistic (data not shown). The time constant of solution change ( $\tau_p = 49.0 \pm 2.2$  s,  $n = 6$ ) was not significantly different than that of the volume decrease during the recovery phase following the exposure to 50% hypoosmotic solution, or in response to 110% solution, 120% solution, and 140% solution (see Table 1). When the time constants of volume decrease in these four sets of experiments were pooled ( $\tau_{dec} = 54.4 \pm 3.4$  s,  $n = 20$ ) they were not statistically different than that of the solution change. In these four sets of experiments (referred to here as Group 1), the time constant of the volume increase in APHCs was found to be consistently larger than the one characterizing volume decrease. A paired two-sample *t*-test showed statistically significant differences between the time constants of volume increase and volume decrease for the 50% ( $p < 0.03$ ), 110% ( $p < 0.05$ ), 120% ( $p < 0.03$ ) and 140% ( $p < 0.02$ ) osmotic challenges (pooled:  $\tau_{inc} = 154 \pm 16.9$  s; ratio =  $3.0 \pm 0.3$ ;  $p < 10^{-5}$ ,  $n = 20$ ). These results suggest that in Group 1 experiments the perfusion rate was the limiting factor in setting the rate of volume decrease in APHCs, while the biophysical properties of the cell membrane had contributed to the longer time constants of volume increase.

For the other osmotic challenges (75–105%, Group 2), however, the time constant of single exponential curve fitted to the volume decrease time course was significantly longer than that of the perfusion system (ANOVA:  $p < 0.02$ , for each case; pooled:  $p < 0.005$ ), and also significantly longer than the time constant of volume decrease in Group 1 ( $p < 10^{-4}$ ). The time constant of volume decrease in Group 2 experiments were, however, not significantly different than the time constant for their corresponding volume increase time course (paired *t*-test). The difference between  $\tau_{inc}$  ( $124 \pm 10.9$  s) and  $\tau_{dec}$  ( $72.2 \pm 4.9$  s) was still significant (ratio,  $2.1 \pm 0.2$ ;  $p < 0.0002$ ,  $n = 39$ ), when corresponding time constants in the two groups were combined. The difference between  $\tau_{inc}$  and  $\tau_{dec}$  was also found to be significant when the data for the hyperosmotic challenges were combined, but not for the hypoosmotic solutions (see Table 1).

### 3.3. Osmotic permeability of APHCs' plasma membrane

In order to determine if the osmolarity- and direction-dependence of time constants presented in Fig. 3B represent the

**Table 1**  
Time constants and Osmotic permeability coefficients

Rel. osmolarity ( <i>n</i> )	Volume decrease		Volume increase		Ratio	
	$\tau$ (s)	$P_f (\times 10^{-3} \text{ cm/s})$	$\tau$ (s)	$P_f (\times 10^{-3} \text{ cm/s})$	$\tau$	$P_f$
50% (5)	56.0 ± 4.0 <sup>a</sup>	20.4 ± 2.7 <sup>b</sup>	151 ± 35.4	9.3 ± 2.5	2.7 ± 0.7	2.7 ± 0.5
75% (5)	97.3 ± 14.3	9.5 ± 0.3	115 ± 17.0	7.9 ± 2.6	1.3 ± 0.2	1.6 ± 0.3
90% (7)	97.6 ± 15.6	13.4 ± 2.1	88.4 ± 12.7	13.2 ± 2.0	1.1 ± 0.2	1.1 ± 0.2
95% (7)	86.5 ± 11.9	11.9 ± 3.8	–	–	–	–
50–95%	85.6 ± 7.0	13.6 ± 1.5	115 ± 13.5	10.5 ± 1.4	1.6 ± 0.3	1.7 ± 0.3
105% (7)	79.8 ± 8.3	15.2 ± 2.3	75.3 ± 12.9	15.8 ± 1.7	1.0 ± 0.2	0.9 ± 0.1
110% (5)	52.4 ± 7.7 <sup>a</sup>	18.9 ± 2.8 <sup>b</sup>	133 ± 32.4	7.6 ± 1.5	2.9 ± 0.8	2.9 ± 0.7
120% (5)	56.7 ± 11.2 <sup>a</sup>	18.0 ± 2.4 <sup>b</sup>	145 ± 29.5	9.5 ± 2.3	2.8 ± 0.7	3.2 ± 1.4
140% (5)	52.4 ± 3.0 <sup>a</sup>	11.1 ± 1.0 <sup>b</sup>	186 ± 43.0	3.8 ± 1.3	3.5 ± 0.7	4.1 ± 1.0
105–140%	62.1 ± 4.7	15.7 ± 1.2 <sup>b</sup>	132 ± 16.5	9.5 ± 1.3	2.5 ± 0.4	2.6 ± 0.5
50–140%	74.4 ± 4.6	14.6 ± 1.0 <sup>b</sup>	124 ± 10.9	9.9 ± 0.9	2.1 ± 0.2	2.2 ± 0.3

Time constants of volume changes recorded in 46 APHCs in response to, and during the recovery from, osmotic changes applied by bath perfusion. Also shown are the osmotic permeability coefficients of these APHCs estimated with the small-signal approximation method (equations (B4) and (B5)). The data is presented as mean ± SEM for each set of osmotic challenges, as well as for the combined 50–95%, 105–140% and 50–140% relative osmolarity.

For the unmarked sets of experiments, the difference between time constants of the volume decrease and perfusion was found to be significant (ANOVA:  $p < 0.02$ ). However, time constants of the volume decrease and volume increase were not significantly different (paired *t*-test:  $p > 0.25$ ).

<sup>a</sup> The time constant of volume decrease was not significantly larger than that of the perfusion system ( $49.0 \pm 2.2$  s,  $n = 6$ ; ANOVA:  $p > 0.13$ , in each case), but significantly smaller than the time constant of its corresponding volume increase (paired *t*-test:  $p < 0.05$ ).

<sup>b</sup> The osmotic permeability coefficient estimated from the volume decrease measurements was significantly larger than the estimated  $P_f$  for their respective volume increase episode ( $p < 0.02$ ).

rectification of osmotic flow in APHCs, the data were rearranged and displayed in accordance with the relationships derived by Zhi et al. (2007) (Fig. 3C), and by Farmer and Macey (1970) (Fig. 3D), for semipermeable membranes. According to Zhi et al. (2007), there exists a linear relationship between the inverse of the time constant ( $b = 1/\tau$ ) of the fitted single exponential to the volume change, and the osmotic difference applied to the cell (see equation (3) in the Methods for the case of cylindrical cells). In Fig. 3C, we have displayed an extended version of this relationship for APHCs where data for the volume changes evoked by both hypoosmotic and hyperosmotic challenges, as well during their withdrawal, are included. According to equation (3), the line fitted to these data points has a slope,  $s = -P_f$ .

The least square regression line fitted to all data points (the solid line in Fig. 3C) had a slope of  $s_{\text{all}} = -6.2 \pm 0.4 \times 10^{-4}$  cm/s (correlation coefficient,  $R = -0.88$ ,  $n = 85$ ). Lines fitted to the data derived from the volume increase time courses ( $s_{\text{inc}} = -4.0 \pm 0.4 \times 10^{-4}$  cm/s,  $R = -0.60$ ,  $n = 39$ ), and to those representing volume decreases ( $s_{\text{dec}} = -8.4 \pm 0.5 \times 10^{-4}$  cm/s,  $R = -0.86$ ,  $n = 46$ ), had significantly different slopes (Student's  $t$ -test:  $s_{\text{all}}$  and  $s_{\text{inc}}$ :  $p < 0.0004$ ;  $s_{\text{all}}$  and  $s_{\text{dec}}$ :  $p < 0.0009$ ;  $s_{\text{inc}}$  and  $s_{\text{dec}}$ :  $p < 0.0001$ ). The line fitted to the data derived from the volume decreases in response to the 105–120% hyperosmotic solution had the steepest slope,  $s = -10.1 \pm 0.8 \times 10^{-4}$  cm/s ( $R = -0.85$ ,  $n = 17$ ; dashed line). However, when the data corresponding to the volume increase during the recovery phase of the same experiments were also included (as in Fig. 2G), the slope of the fitted line ( $s = -7.6 \pm 0.7 \times 10^{-4}$  cm/s,  $R = -0.91$ ,  $n = 34$ ) became significantly shallower ( $p < 0.02$ ; not shown). The data points corresponding to the volume decreases in Group 1, were fitted with a line of slope,  $s = -9.0 \pm 0.7 \times 10^{-4}$  cm/s,  $R = -0.80$ ,  $n = 20$  (not shown).

These results suggest that inclusion in the analysis of the data derived from the time course of recovery after an osmotic shock did not significantly alter the estimated osmotic permeability. However, the  $P_f$  calculated by this approach clearly reflects the direction dependence observed in both the extent of volume changes (Fig. 2F), as well as in the response kinetics (Fig. 3B). In order to determine if this direction dependence depicts rectification of osmotic flow, we adopted the approach originally devised by Farmer and Macey (1970). Using the Taylor series expansion of Van't Hoff's law, and linearization of the series for small changes in the volume and osmolarity, these authors showed that the time constant of osmotically-induced volume change,  $\tau \propto \pi^{-2}$ , where  $\pi$  is the relative osmolarity of the test solution ( $=C(\infty)/C(0)$ ). As we have stated in the Methods equation (4), this relationship can be written in the form,  $(\kappa\tau)^{-1} = P_f \pi^2$ , where  $\kappa = V_W A C_0 / \phi V_0$ . For membranes permeable only to water,  $\kappa$  is a constant determined by the cell's initial characteristics in the iso-osmotic solution. However, it appeared possible to obtain a reasonable fit to this relationship for membranes with limited permeability to solutes if  $\kappa$  is calculated for the initial condition of the cell at the onset of every osmotic challenge, and  $\pi$  is taken as the final osmolarity of the solution normalized with respect to the osmolarity of the bathing medium at the start of the osmolarity change.

In Fig. 3D, we have shown the relationship between  $(\kappa\tau)^{-1}$  and  $\pi^2$  for the data in Fig. 3B. Accordingly, the slope of the least squares regression line fitted to the data in this figure can be taken as the osmotic permeability coefficient ( $P_f$ ) of these APHCs. The solid line fitted to all data points in Fig. 3D has a slope of  $P_f = 6.9 \pm 0.3 \times 10^{-4}$  cm/s ( $R = 0.77$ ,  $n = 85$ ). For osmotic changes inducing volume increase (data points with  $\pi^2 < 1$  in Fig. 3D),  $P_f = 8.2 \pm 0.7 \times 10^{-4}$  cm/s ( $R = 0.43$ ,  $n = 39$ ); while for those causing shrinkage ( $\pi^2 > 1$  in Fig. 3D), the slope was  $P_f = 6.8 \pm 0.4 \times 10^{-4}$  cm/s ( $R = 0.73$ ,  $n = 46$ ). The differences between these estimates of the osmotic permeability coefficient are, however, not statistically

significant. However,  $P_f$  estimated from the volume decreases in response to the 105–120% osmolarity ( $8.9 \pm 0.8 \times 10^{-4}$  cm/s,  $R = 0.35$ ,  $n = 17$ ), and from both volume decreases and increases in the same experiments ( $8.5 \pm 0.6 \times 10^{-4}$  cm/s,  $R = 0.62$ ,  $n = 28$ ) were significantly different than the one estimated from fitting all data points at once ( $p < 0.020$  and  $p < 0.021$ , respectively). Thus, at variance with the osmotic coefficients estimated on the basis of method of Zhi et al. (2007), the  $P_f$  calculated by utilizing the approach devised by Farmer and Macey (1970) is direction- and osmolarity-independent, suggesting that osmotic water flow across the membrane of APHCs is not rectified.

The small magnitude of  $P_f$ s estimated by aforementioned methods clearly shows that in our perfusion experiments, one or both underlying assumptions of these methods, namely a semi-permeable membrane and instantaneous solution change have been compromised. To minimize the error in the estimate of the osmotic permeability coefficient due to solute permeability and slow perfusion, we applied Van't Hoff's law to the volume changes at the onset of each osmotic challenge (equations (B4) and (B5)). As shown in Fig. 5B, this group of estimates for  $P_f$  in 46 experiments (85 volume-change experiments) covered a wide range (from 1.3 to  $33.0 \times 10^{-3}$  cm/s), possibly because of the variations in the calculated time constants. However, the average  $P_f$  estimated on the basis of this method,  $12.5 \pm 0.7 \times 10^{-3}$  cm/s ( $n = 85$ ), is 18–20 times our estimates made with the other two methods (see Table 1, for the mean and SEM of  $P_f$  for each set of experiments). The  $P_f$  estimated for the volume decrease measurements is  $14.6 \pm 1.0 \times 10^{-3}$  cm/s ( $n = 46$ ; range, 1.6– $33.0 \times 10^{-3}$  cm/s), and for the 105–120% hyperosmotic challenges, for which  $\phi = 0.88$  (Fig. 2F), is  $17.1 \pm 1.4 \times 10^{-3}$  cm/s ( $n = 17$ ; range 8.7– $27.6 \times 10^{-3}$  cm/s). The  $P_f$  estimated for the volume decrease in Group 1 experiments is  $17.1 \pm 1.3 \times 10^{-3}$  cm/s ( $n = 20$ ; range, 9.0– $27.6 \times 10^{-3}$  cm/s). These latter two estimates are not significantly different, but they are both significantly larger than the average  $P_f$  ( $p < 0.01$ , and  $p < 0.006$ , respectively). Volume increases for these two groups of experiments yielded significantly smaller estimates than those obtained from their respective volume decrease data ( $11.3 \pm 1.4 \times 10^{-3}$  cm/s,  $p < 0.006$ ; and  $7.6 \pm 1.0 \times 10^{-3}$  cm/s,  $p < 10^{-5}$ , respectively). These results suggest that data from those experiments in which solute transport is minimum ( $\phi = 0.88$ ), or the rate of volume change is comparable with that of the perfusion (Group 1), yields significantly larger estimates of  $P_f$ . Furthermore, our results suggest that the 'small-signal' approximation method is applicable to osmotically-induced volume changes, particularly when solute flow across the cell membrane is negligible (see Discussion).

These considerations led us to devise experiments in which (a) osmotic challenges were applied rapidly, and (b) to generate hyperosmolarity, sucrose was added as an impermeable solute to the bathing solution (Echevarria and Verkman, 1992). Fig. 4A shows the rapid shrinkage of six APHCs – with different initial volumes – in response to the injection of 2  $\mu$ l of 1.5 M sucrose in 100 ms into the 500- $\mu$ l recording chamber (see Fig. 1C and D, and Methods for the description of the injection setup). The transient volume decrease could be fitted with the sum of two exponential curves. The shorter time constants for the examples in this figure were 4.8, 4.8, 5.4, 9.0, 10.9 and 17.4 s ( $8.7 \pm 2.0$  s). Fig. 4B shows these same volume changes normalized, while Fig. 4C shows the mean  $\pm$  SEM of the normalized volume changes along with the least squares fit of the mean to the sum of two exponentials. The fitted curve had time constants 6.7 s and 88.5 s.

In Fig. 4D, we have superimposed the results of six groups of similar experiments in which 2  $\mu$ l of 0.25, 0.5, 1 or 1.5 M, or 5  $\mu$ l of 1 or 1.5 M sucrose were injected into the recording chamber. Each curve shown is the mean of 4–8 similar experiments. Also shown is the sum of two exponentials fitted to each mean curve and its

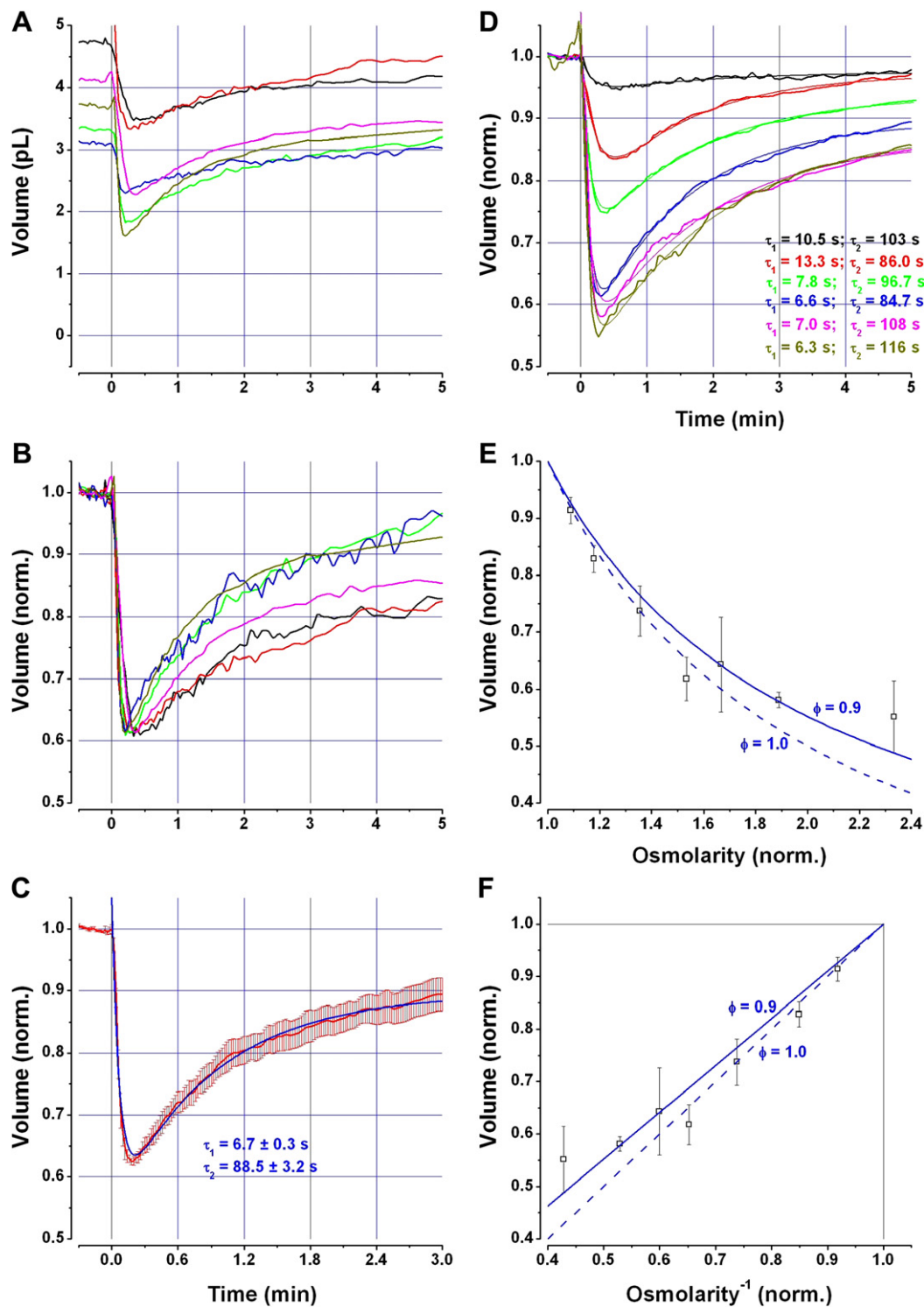


**Fig. 4.** Rapid volume changes in APHCs generated by the injection of hyperosmotic sucrose. A: six sample time courses of APHCs' responses to the injection of 2  $\mu$ l of 1.5 M sucrose. B: the responses in A normalized. C: the average and SEM of the normalized responses in B. D: from top to bottom, the average responses to the injection of 2  $\mu$ l of 0.25 M, 0.5 M, 1.0 M and 1.5 M sucrose, and 5  $\mu$ l of 1.0 M and 1.5 M sucrose. Each curve shown is the mean of 4–8 similar experiments. Also shown is the sum of two exponentials fitted to each mean curve and (from top to bottom) their respective time constants. E: the volume vs. osmolarity relationship for the data collected in the injection experiments. The solid curve fitted to these data represents the Boyle–Van't Hoff law (equation (2)). The dashed line is the same equation with  $\phi = 1$ , showing a reasonable fit to the data points for which normalized osmolarity  $\leq 1.5$ . F: the solid line fitted to the volume vs. the inverse of osmolarity relationship has a slope,  $\phi = 0.9$ , while the data for the smaller hyperosmotic levels can be fitted with a (dashed) line with a slope closer to 1.0.

respective time constants. Injection of hypoosmotic solutions, or even pure water failed to produce any measurable volume change (data not shown). Fig. 4E shows the osmolarity–volume relationship for these groups of experiments, along with the Boyle–Van't

Hoff curve fitted to the data (solid line). The dashed line in this figure shows that when small hyperosmotic challenges (up to 150%) are rapidly applied to APHCs, they behave as ideal osmometers with  $\phi = 1$ . The linear relationship between the normalized volume

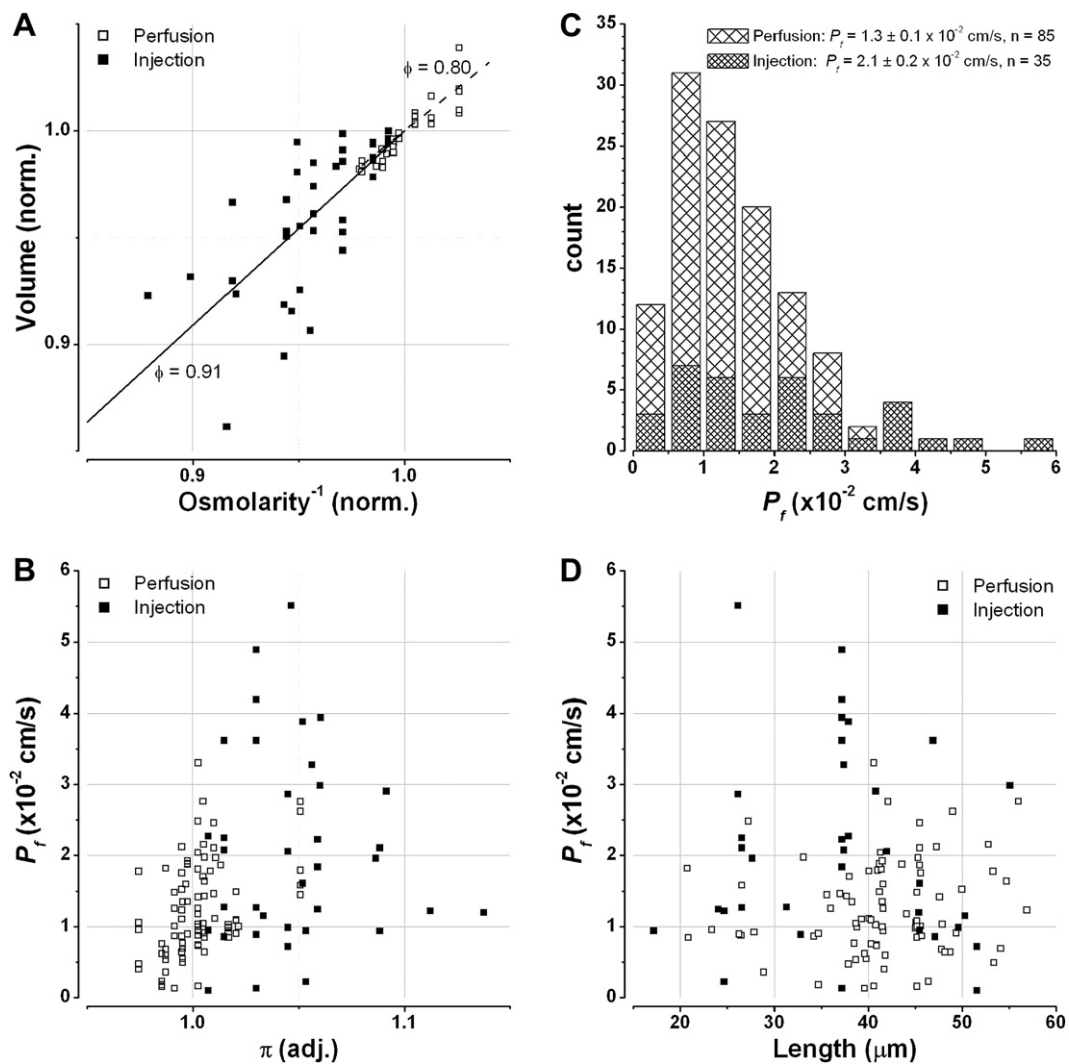


**Fig. 5.** ‘Small-signal’ shape change in APHCs. A: the volume vs. the inverse of osmolarity at the first time point ( $t = 5$  s, for perfusion;  $t = 1$  s, for injection) after the start of solution change. Extracellular osmolarity was assessed from the time course of the solution change (Fig. 1B and D). The ‘small-signal’ data for the perfusion experiments (open squares), and the dashed line fitted to these data points are also shown. B: ‘small-signal’ estimate of the osmotic permeability coefficient as a function of external osmolarity (adjusted = normalized with respect to the osmolarity at  $t = 0$ ). For comparison, both estimates of  $P_f$  from the injection (closed squares) and perfusion experiments (open squares) are shown. C: histogram of the estimated osmotic permeability coefficients derived from 35 measurements with the injection device (fine hachure), and 85 measurements with the perfusion system (coarse hachure). D: distribution of the osmotic permeability coefficients as a function of the APHC’s initial length.

change and the inverse of osmolarity is shown in Fig. 4F. As a corollary to these results, we suggest that, (a) the osmotically inactive fraction of APHCs is at most about 10% of their isoosmotic volume, and (b) as in many other cell membranes, permeability of APHCs to sucrose is very limited.

Lack of permeability to sucrose will prevent this agent from crossing the membrane to diminish the osmotic gradient. However, even in the absence of a measurable permeability to sucrose, any volume decrease in response to a hyperosmotic challenge will increase the outward gradient for permeable intracellular solutes. Therefore, it is conceivable that volume changes shown in Fig. 4 are mitigated by the outflow of such solutes. In order to minimize the impact of such underestimation of the volume change, we used the ‘small-signal’ response of APHCs to osmotic changes in the same manner employed before for calculation of the osmotic permeability for perfusion experiments summarized in Table 1 (and shown in Fig. 5B). Fig. 5A shows the volume vs. inverse osmolarity relationship at the onset of response to osmotic changes applied through the perfusion system (open squares), as well as that for the

hyperosmotic injections shown in Fig. 4 (solid squares). Also shown is the Boyle–Van’t Hoff’s line (equation (2) in Methods), fitted to these data.

Fig. 5B shows the osmotic permeability coefficients calculated on the basis of the data collected with the fast injection setup and hyperosmotic extracellular solution containing sucrose (solid squares). Also shown for comparison are  $P_f$ s calculated for APHCs in experiments utilizing the perfusion system (open squares). As the histogram in Fig. 5C shows, the use of a rapid injection system made only a modest increase in the estimate of  $P_f$  for the APHCs compared with that possible with the slower perfusion setup. In fact, while the difference between the  $P_f$  obtained by the use of injection system ( $20.6 \pm 2.3 \times 10^{-3}$  cm/s,  $n = 35$ ), and the average  $P_f$  estimated from the perfusion data ( $12.5 \pm 0.7 \times 10^{-3}$  cm/s,  $n = 85$ ) is significant (ANOVA:  $p < 10^{-4}$ ), its difference with the  $P_f$  for the volume decrease in response to 105–120% solutions ( $17.1 \pm 1.4 \times 10^{-3}$  cm/s), or in the Group 1 experiments ( $17.1 \pm 1.3 \times 10^{-3}$  cm/s), is not. Lastly, the osmotic permeability coefficient in APHCs appears to be independent of the cell’s length (Fig. 5D).

3.4. The effects of mercury on APHCs' osmotic permeability

Mercurial compounds are known to block several types of water channels (aquaporins) in mammalian cell membranes (Ishibashi et al., 2009). In order to determine whether a mercury-sensitive water channel mediates the relatively high permeability of APHCs to water, we tested the effect of a high concentration (0.5 mM) of HgCl<sub>2</sub> on the osmotically-induced volume change in these cells. Mercuric chloride, on its own, caused a conspicuous shape change in APHCs, composed of an initial transient expansion followed by a sustained contraction (Fig. 6). In seven APHCs treated with 0.5 mM HgCl<sub>2</sub>, the length initially increased by a significant  $1.4 \pm 0.4\%$  ( $p < 0.016$ ), before shortening to  $95.0 \pm 1.3\%$  of its original level in 5 min ( $p < 0.012$ ). As shown in Fig. 6A, shortening persisted for at least 25 min after the washout of HgCl<sub>2</sub>. The transient volume increase was also significant ( $5.6 \pm 1.3\%$ ,  $p < 0.009$ ), which was followed by shrinkage to  $89.6 \pm 1.5\%$  of the peak volume ( $p < 0.001$ ) by the end of the 5-min treatment with HgCl<sub>2</sub>.

In all APHCs exposed to mercury, removal of the inhibitor from the medium led to cell swelling. Another consistent feature of mercury-treated APHCs was the formation of one or two membrane

blebs. Fig. 6B shows the cell in Fig. 6A at 11, 14 and 17 min after the start of recording. During this 6-min period, the rate of increase in the volume of the bleb was, in average, six times that of the cell soma. As shown in Fig. 6A, from 17 min on, the volume of this APHC's soma (open squares) no longer increased, while its length (filled squares) continued to shorten. Thenceforth, the bulk of the increase in the total volume (open circles) in this, and all other APHCs similarly treated with mercury, was confined to the bleb(s). It is of interest that when this APHC was exposed to an osmotic challenge (e.g., 110% osmolarity, between 20 and 25 min after the start of recording in Fig. 6A), it was still capable of displaying a typical volume change.

Fig. 6C shows the response of an APHC to a hypoosmotic challenge (90% osmolarity), before, during, and after treatment with 0.5 mM HgCl<sub>2</sub>. As expected, under control conditions, lowering the extracellular osmolarity by 10% increased the cell's volume and decreased its length. After the 5-min treatment with mercuric chloride, the same challenge increased both volume and length. Following a 10-min washout with the AP solution without the inhibitor, the response to the 90% osmolarity was qualitatively similar to the control, despite significant mercury-induced changes

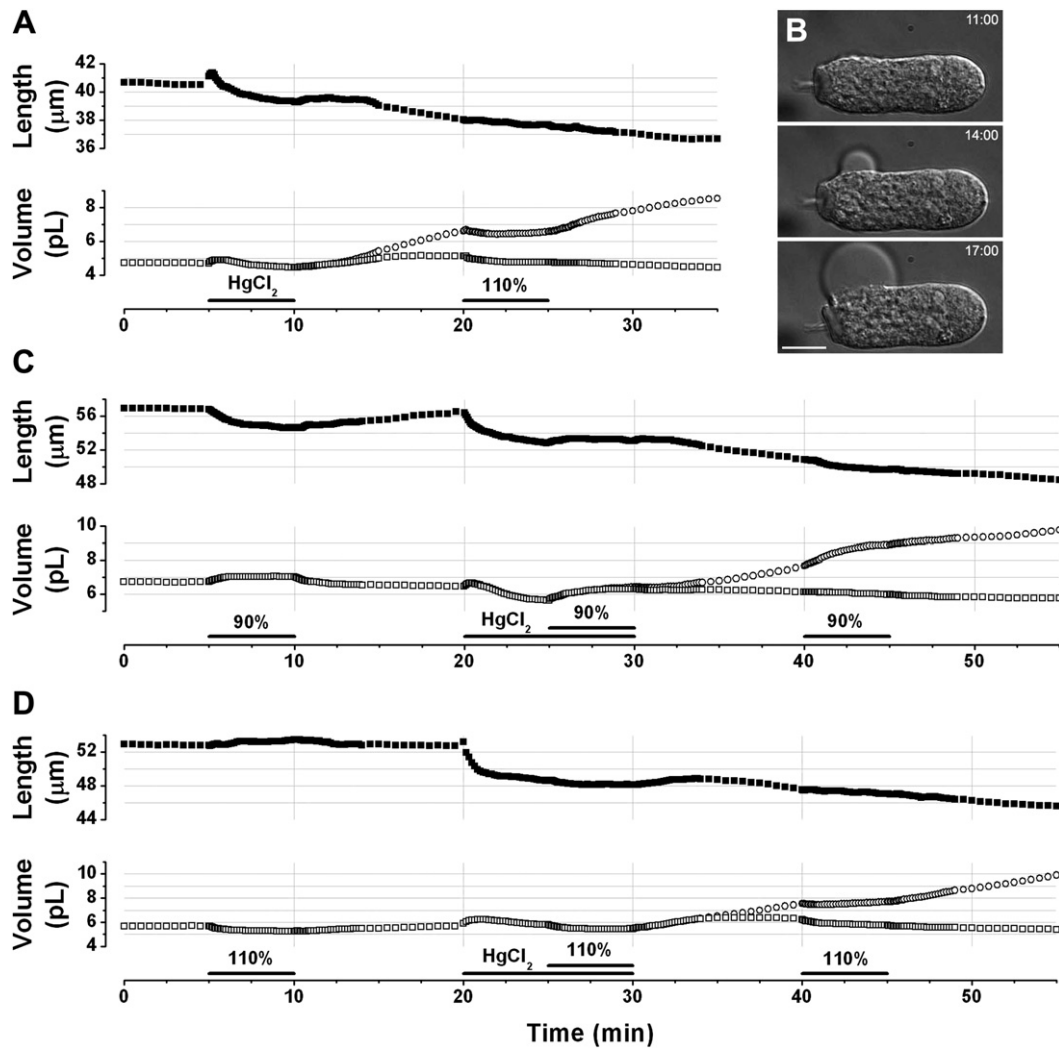


**Fig. 6.** The effects of mercuric chloride. A: 0.5 mM HgCl<sub>2</sub> causes a shape change in APHCs composed of a transient increase in the cells' length and volume, followed by a sustained shortening and shrinkage. Removal of mercury from the medium leads to cell swelling and further shortening. B: The bulk of the increase in the total volume (open circles in A, C and D), was confined to one or two blebs. C: HgCl<sub>2</sub>-treated APHCs, however, respond to a 10% reduction in the osmolarity with features (extent and time constant of swelling, as well as estimated  $P_f$ ) that are not significantly different than those of the control measurements. During the washout period, APHCs equally respond to the hypoosmotic challenge. D: The characteristics of the response to the 110% hyperosmotic solution is also unaffected by the treatment with 0.5 mM HgCl<sub>2</sub>.

in the cell's length and volume. In a total of three similar experiments, the hypoosmotically-induced volume increase in the presence of mercury ( $9.3 \pm 1.5\%$ ) was not significantly different than the response under control conditions ( $6.6 \pm 1.5\%$ ; paired *t*-test). The difference in the length changes was, however, significant ( $+0.3 \pm 1.1\%$  in the mercury-treated cells vs.  $-3.7 \pm 0.3$  under control conditions,  $p < 0.021$ ). After 10 min of wash, a 10% decrease in the osmolarity produced a  $3.3 \pm 0.7\%$  decrease in the length, and a  $13.2 \pm 2.6\%$  increase in the volume, which were not statistically different than their respective controls. It was noted that these changes in the length and volume might have been exaggerated by the ongoing mercury-induced shape change. Neither the time constant of 90% osmolarity-induced volume increase ( $89.3 \pm 20.9$  s) nor the osmotic permeability coefficients ( $33.7 \pm 10.5 \times 10^{-3}$  cm/s) in mercury-treated cells were significantly different than their respective control values ( $93.2 \pm 20.0$  s and  $16.0 \pm 3.9 \times 10^{-3}$  cm/s, respectively).

The effects of mercury on the shape change induced by hyperosmotic solutions were also examined in three APHCs. Fig. 6D shows an example. As we have stated earlier (see Fig. 2C and D), hyperosmotic solutions do not change the APHC's length significantly. Mercury treatment did not alter this lack of effect (control:  $-2.2 \pm 1.5\%$ ; treated:  $-1.6 \pm 0.7\%$ ). The volume decrease produced by the 110% osmolarity ( $7.7 \pm 1.7\%$ ), was also not changed significantly by 0.5 mM HgCl<sub>2</sub> ( $6.5 \pm 2.3\%$ ). The time constant of the volume decrease in these cells in response to 110% osmolarity ( $45.6 \pm 3.0$  s), was not significantly modified by mercury ( $44.3 \pm 1.3$  s). Therefore, the estimated osmotic permeability coefficients of these APHCs were also unaltered by this agent (control:  $21.7 \pm 5.5 \times 10^{-3}$  cm/s; treated:  $17.9 \pm 4.8 \times 10^{-3}$  cm/s). Because of the mercury-induced swelling of APHCs, quantitative comparison of time constants of the recovery phase of the response to the 110% osmolarity, or the response to that osmotic challenge after the washout of HgCl<sub>2</sub>, with that of the control was not feasible. For the same reason, the estimated *P*<sub>s</sub> for this period were not compared with control.

In summary, while a high concentration of HgCl<sub>2</sub> produces a shape change in APHCs that is somewhat reminiscent of that induced by ionomycin (Farahbakhsh and Narins, 2006, 2008), its effects on the osmotically evoked shape change and on the permeability to water in these cells are not statistically significant.

#### 4. Discussion

When faced with gradual decreases in the extracellular osmolarity, APHCs exhibit a conspicuous capacity for minimizing both the extent and speed of the expected volume increase, while conversely acting as an almost ideal osmometer when exposed to modestly hyperosmotic media. Large increases in the extracellular osmolarity, however, cause cell membrane indentation and collapse, as previously observed in OHCs (Chertoff and Brownell, 1994). In contrast with OHCs (Ratnanather et al., 1996; Zhi et al., 2007), APHCs' response to an osmotic challenge is generally reversible, and in most cases reproducible. This latter property allows one to investigate the directional sensitivity of osmotically-induced volume changes—and thus, possible rectification of water flow—independent of the osmotic challenge's initial and final levels, as long as the equilibrium condition can be ascertained for the starting point.

The asymmetrical nature of responses to osmotic challenge has led us to conclude that (a) APHCs' cytoplasmic membrane cannot be regarded as semipermeable, i.e., only permeable to water; and hence (b), any attempt to use the size of the volume change induced by hypoosmotic solutions for calculating the osmotic permeability coefficient of this membrane will produce an underestimate.

Similarly, estimates based on the data gathered in response to relatively large increases in osmolarity would be inaccurate. A further complicating factor is the relatively slow rate of bath perfusion, which turned out to be the limiting factor for measuring some of the osmotically induced volume decreases. Combined with the membrane permeability to solutes, slow perfusion will help dissipate the transmembrane osmotic gradient diminishing the driving force for water movement. As a result, our estimate of the APHCs' osmotic permeability assuming a semipermeable membrane and an stepwise (instantaneous) solution change, while three times (Fig. 3C and D) that estimated for OHCs (Ratnanather et al., 1996; Zhi et al., 2007), is still smaller by an order of magnitude than that obtained when we took these mitigating factors into consideration (Fig. 5B).

##### 4.1. Membrane permeability to solutes

As we show in Appendix A, if the cell membrane is permeable to intracellular solutes, lowering the extracellular osmolarity will induce an outward flow of permeable solute(s) proportional to the applied osmotic change. This outward flow diminishes the transmembrane gradient for water, and thus reduces the extent of volume increase. When the membrane solute permeability is high and the osmolarity change is relatively slow, there may be no volume change at all — 'isovolumetric' response, as in Fig. 2B. In the classical regulatory volume decrease (RVD) seen in many cell types, the membrane permeability for some intracellular ions or non-electrolytes is increased by a stretch-sensitive mechanism (Hoffmann et al., 2009). In the absence of a gross volume change (as in Fig. 2B), and, therefore, a significant change in the intracellular osmolarity and ionic strength, activation of an osmo- or stretch-sensitive mechanism appears unlikely. However, it is still plausible to suggest that an osmosensor operating in the APHC's membrane microdomains may still change the membrane's local permeability to the solute.

For a 5% change in the extracellular osmolarity, the pressure change across the membrane — at most, 0.273 atm., or 208 mmHg (equation (B3), for  $\sigma = 1$ ) — should be sufficient to trigger such a permeability increase. Alternatively, 5% dilution of the extracellular medium may provide enough of a gradient for the solute movement through existing pathway(s). In the latter case, the solute is assumed to be at chemical equilibrium before the osmotic challenge is initiated. A combination of these two osmotically induced changes (i.e., in the gradient and permeability) are also possible. We attribute this reduced volume—change response to hypoosmotic solutions to the presence of an 'immediate' RVD, in contrast to the classical RVD which is usually delayed and is triggered by significant increase in volume. APHCs also exhibit a classical RVD, however, after a delay of  $383 \pm 51$  s (for a 50% osmolarity decrease; unpublished observations).

The isovolumetric response to an osmotic challenge (as in Fig. 2B) has previously been observed in OHCs. However, it was attributed to the ability of the cell's hydraulic skeleton to maintain its shape despite slow changes in osmolarity (Chertoff and Brownell, 1994). APHCs do not exhibit electromotility (unpublished observation), and may not express prestin (Manley, 2000). Furthermore, they appear to lack subsurface cisternae (D.D. Simmons, personal communication). As a result, their lateral membrane appears more similar to that of IHCs than OHCs. For these reasons, we consider any mechanical effect of the APHCs' cytoskeleton as negligible (see also Ratnanather et al., 1996). In what is termed "isovolumetric regulation" (IVR, Lohr and Grantham, 1986), a rather slow rate of change in the extracellular osmolarity is tolerated without a measurable volume change by cells in the rabbit kidney proximal tubule (Lohr and Grantham,

1986; Lohr, 1990), toad distal tubule cell line, A6 (Van Driessche et al., 1997; Grosse et al., 2001), rat C6 glioma cells (Lohr and Yohe, 2000), chick embryonic cardiomyocytes (Souza et al., 2000), and by rat hippocampal slices (Quesada et al., 2000).

#### 4.2. Osmotic permeability coefficient of APHCs

The 'small-signal' approach (Appendix B) allowed us to obtain estimates of  $P_f$  (Fig. 5B) that are much larger, and in our view more realistic, than those based on equations (3) and (4) (Fig. 3C and D). However, the validity of such assumptions needs to be tested. As we have summarized in Table 1 and briefly described in the Results, for moderate increases in osmolarity, when the concentration of all components of the extracellular medium (AP solution) is kept constant and hyperosmolarity is produced by addition of a membrane-impermeant solute (sucrose), APHCs acted as ideal osmometers (with  $\phi = 0.88$ ). In other words, their membrane appeared only permeable to water, at least until cell shrinkage significantly changed the gradient for intracellular solutes. Therefore, for these close-to-ideal conditions, the small-signal method produced an estimate of the osmotic permeability coefficient that was large and had only a small error ( $17.1 \pm 1.4 \times 10^{-3}$  cm/s). Thus, it appears that for these measurements, the assumptions for the equations (B1) and (B2) were valid:  $\sigma RT\Delta c_s$  was small compared with  $\Delta p$ , and its changes followed the same time course as the solution change (for these responses the time constant of volume change was not statistically different than that of solution change). Despite reversibility of these responses (Fig. 2G), time constants of the recovery period were large and quite variable (Table 1) producing a statistically smaller estimate of  $P_f$  ( $11.3 \pm 1.4 \times 10^{-3}$  cm/s; paired  $t$ -test:  $p < 0.01$ ). Thus, for the recovery period, the assumptions of equations (B1) and (B2) were not valid. Since the loss of intracellular solute was insignificant ( $\phi = 0.86$ ), the slow pace of recovery in these experiments was unexpected. Some of the recovery phases were also preceded by significant delay. Therefore, we suspect that apparent delays and large time constants might be caused by cell's partial collapse during the preceding shrinkage (Chertoff and Brownell, 1994), and the failure of our volume estimation method which is most accurate when the cell's transverse cross-section is circular. However, it should be noted that the effect of such collapse on the calculated volume is less than 30% (Fig. 2F), and on the estimated  $P_f$ , less than 40% (Table 1).

Our estimates of  $P_f$  on the basis of volume changes produced by 50–90% osmolarity were also comparatively small and variable ( $10.5 \pm 1.4 \times 10^{-3}$  cm/s; Table 1). We attribute these results to the large efflux of intracellular solutes during this period, and changes in  $\sigma RT\Delta c_s$  which could no longer be in accord with the prerequisites for equations (B1) and (B2). A somewhat larger estimate was obtained when volume changes during the recovery period of these experiments were used ( $14.8 \pm 1.6 \times 10^{-3}$  cm/s). The difference between these two estimates was statistically significant (paired two-sample  $t$ -test:  $p < 0.024$ ). Furthermore, this latter estimate was not significantly different than the  $P_f$  estimated from volume decreases induced by 105–120% osmolarity. These results led us to conclude that the most reliable estimate of  $P_f$  could be obtained when (a) the solute movement across the membrane was minimized, and (b) the rate of solution change in the vicinity of cells was significantly increased. To that end we injected membrane-impermeable sucrose into the recording chamber toward APHCs, as described in Methods (Fig. 1C and D). The results of these experiments (Fig. 4) showed that under these conditions APHCs acted as ideal osmometers ( $\phi = 0.91$ ), with negligible permeability to solutes.

As expected, faster exposure of APHCs to hyperosmotic solutions engendered a small-signal estimate of  $P_f$  ( $20.6 \pm 2.3 \times 10^{-3}$  cm/s),

which was significantly larger than the average  $P_f$  obtained from perfusion experiments ( $12.5 \pm 0.7 \times 10^{-3}$  cm/s, ANOVA:  $p < 10^{-4}$ ), including the one resulting from the volume decreases produced with perfusion ( $14.6 \pm 1.0 \times 10^{-3}$  cm/s,  $p < 0.012$ ), but not the one calculated for the volume decrease in response to 105–120% osmolarity solutions ( $17.1 \pm 1.4 \times 10^{-3}$  cm/s), or in Group 1 experiments ( $17.1 \pm 1.3 \times 10^{-3}$  cm/s). Furthermore, the difference in the  $P_f$  estimates obtained by the perfusion and injection systems in our experiments was not as great as has been noted in mammalian OHCs (Zhi et al., 2007). According to these authors, injection of a viscous solution through a small orifice (radius,  $R$ ), positioned at a distance,  $H$  from the cell will produce a wall pressure and shear stress away from the point of impact, within a concentrated region of about  $3R$ . When  $H/R = 4$ –60, such an impact causes strain-dependent osmotic water transport across the cell membrane via selective mechano-sensitive pores (Zhi et al., 2007). Such a thesis may be reasonably applicable to a small-radius ( $R = 0.5$ – $2.5$   $\mu\text{m}$ ) pipette placed near a cell ( $H = 10$ – $30$   $\mu\text{m}$ ), for which  $3R$  covers only a fraction of the cell surface area. In the injection system we used,  $R = 0.19$  mm and  $H = 5$  mm. Thus, an  $H/R = 26$  falls in the middle of the range defined by Zhi et al. (2007). However, the area of impact ( $3R = 0.57$  mm) is much larger than the size of an APHC, and, therefore, the injected solution will not appear to the cell much different than the pressure-gradient flow during bath perfusion. Therefore, it is unlikely that a local wall pressure and shear stress is created on the APHC membrane. A possible exception might be a very small region near the cell margin whose contribution to the whole-cell osmotic permeability is minimal. The rather modest difference between our estimates of the APHCs' osmotic permeability coefficient obtained with the perfusion and injection systems leads us to suggest that the large  $P_f$  in these cells (in the  $10^{-2}$ -cm/s range) requires the presence of water channels in the plasma membrane.

#### 4.3. The effects of mercuric chloride

Despite its rather conspicuous effect on the APHC's shape, 0.5 mM  $\text{HgCl}_2$  appeared ineffective in modifying the osmotic permeability of the cytoplasmic membrane in these cells: neither the extent nor kinetics of osmotically-induced volume changes in  $\text{Hg}^{2+}$ -treated cells appeared significantly different than their respective untreated controls. These results suggest that water movement through the membrane is via a pathway insensitive to extracellular mercury. In some instances, however, in particular in response to hypoosmotic solutions, it appeared that volume increase was larger in the  $\text{Hg}^{2+}$ -treated than in control, suggesting possible inhibition of the solute transport by mercury. However, because of the overlapping  $\text{Hg}^{2+}$ -induced swelling the significance of such an increase could not be established.

### 5. Summary and conclusion

A cell's rather large ( $>10^{-2}$  cm/s) osmotic permeability coefficient is taken as an indication of the expression of functional water channels (aquaporins) in its plasma membrane (Verkman, 1989). Extracellular mercuric compounds inhibit eight of the ten aquaporins known to be expressed in the cytoplasmic membrane (Ishibashi et al., 2009); the two exceptions are AQP-4 water channel and aquaglyceroporin, AQP-7. They have both been suggested to be present in anuran amphibians (Suzuki and Tanaka, 2009). Our immunohistochemical studies suggest that AQP-4 is present in AP and saccular hair cells of *R. pipiens* (Miller et al., 2010). AQP-4, possibly the oldest water channel in vertebrates (Nishimoto et al., 2007), is of particular interest – it has the highest single-channel water permeability among aquaporins ( $24 \pm 0.6 \times 10^{-14}$  cm<sup>3</sup>/s;

Yang and Verkman, 1997). Our estimated values for the osmotic permeability coefficient (0.017 or 0.021 cm/s) then would require 700 or 850 AQP-4 monomers per square micrometer of APHCs, in agreement with earlier predictions (Yang and Verkman, 1997).

Unlike terrestrial dwellers amphibious anurans such as *R. pipiens* are unable to maintain their body fluid homeostasis when on dry land: they are vulnerable to dehydration caused by cutaneous evaporative water loss, and their mesonephros kidneys lack the urine-concentrating prowess of mammalian and avian nephrons (Bentley, 2002). However, they are able to tolerate significant water loss (up to 37%) without severe nervous system function (Hillman, 1980). There is no information about changes in the volume and osmolarity of perilymph in amphibians experiencing dehydration–rehydration episodes. However, it has been reported that the threshold for auditory-evoked potentials in the brainstem of *R. pipiens* remains stable when subjected to up to 33% dehydration (Carey and Zelick, 1993). High permeability to water and osmolytes confers to amphibian auditory hair cells the adaptive advantage to endure and compensate for large but gradual changes in the extracellular osmolarity, and thus maintain their physical shape and functional integrity, an ability not yet demonstrated in their mammalian counterparts.

#### Acknowledgements

This work was supported by National Institutes of Health Grant DC-00222.

#### Appendix A. Membrane permeability to solutes

The rate of flow of water,  $J_v$ , and solute,  $J_s$ , across a biological membrane permeable to both water and a (non-electrolyte) solute,  $s$ , when subjected to a hydraulic pressure difference,  $\Delta p$ , is given by (Kedem and Katchalsky, 1958):

$$J_v = L_p(\Delta p - \sigma RT\Delta c_s) \quad (A1)$$

$$J_s = \omega RT\Delta c_s + (1 - \sigma) c_s J_v \quad (A2)$$

where,  $L_p$  is the hydraulic conductivity of the membrane for water ( $=V_w A P_f / RT$ );  $\sigma$ , the reflection coefficient for the solute;  $R$ , the gas constant;  $T$ , absolute temperature;  $\Delta c_s = c_s^0 - c_s^i$ ;  $\omega$ , the mobility of the solute; and  $c_s = \Delta c_s / \ln(c_s^0/c_s^i)$ . For the experiments reported here,

$$\Delta p = RT\Delta C \quad (A3)$$

where,  $\Delta C$  is the osmotic change produced by solution change. In a special case, where the application of an osmotic difference,  $\Delta C$ , does not produce a change in the volume (isovolumetric response, as in Fig. 2B), we will have  $J_v = dV/dt = 0$ . Therefore, from equations (A1) and (A2),

$$\Delta p = \sigma RT\Delta c_s \quad (A4)$$

$$J_s = \omega RT\Delta c_s \quad (A5)$$

Combining equations (A3)–(A5), we will have,

$$J_s = (\omega/\sigma)RT\Delta C \quad (A6)$$

This latter equation indicates that for the cell volume to remain constant an outward solute flow ( $J_s$ ) must be generated proportional to the imposed osmotic change ( $\Delta C$ ). Furthermore, for time-invariant  $\omega$  and  $\sigma$ ,  $J_s$  will have the same time course as  $\Delta C$  (e.g., as in Fig. 1). Finally, for a given  $\Delta C$ , a larger mobility, or a smaller reflection coefficient for the solute causes a faster depletion of the

intracellular solute, and, therefore, an earlier termination of the isovolumetric response.

#### Appendix B. Small signal estimation of $P_f$

For a semipermeable membrane hydraulic conductivity ( $L_p$ ) and osmotic permeability coefficient ( $P_f = RTL_p/AV_w$ ) can be calculated from equation (A1) with the proviso,  $\sigma = 1$ . Contribution of any impermeant solute gradient ( $\Delta c_s$ ) will be a constant that can be accounted for –  $L_p$  is the slope of the linear relationship between applied  $\Delta p$  and measured  $J_v$ . However, for membranes with non-zero permeability for solute(s) ( $\omega > 0$ ;  $1 > \sigma > 0$ ), contribution of  $\sigma RT\Delta c_s$  can be significant, and variable. As a result, depending on the dynamic of osmotically-induced changes in  $\sigma$  and  $\Delta c_s$ , the effective driving force for water movement (i.e.,  $\Delta p - \sigma RT\Delta c_s$ ) may be much smaller than the intended one ( $\Delta p$ ). This appears to be the case for the experiments reported here. The problem was further exacerbated by the fact that solution change was gradual, and not stepwise as intended. Therefore, a more accurate estimation of  $L_p$  (or  $P_f$ ) would require (a) using a more realistic measure of  $\Delta p$ , and (b) minimizing the effects of variations in  $\sigma RT\Delta c_s$ .

To address these issues we made two assumptions: (a), that based on the kinetics of solution change in the vicinity of an APHC (Fig. 1),  $\Delta p = \Delta p^\infty (1 - e^{-t/\tau_p})$ , where  $\Delta p^\infty$  is the intended osmotic pressure change, and  $\tau_p$  is the time constant of the solution change (47.5 s); (b), for very small values of  $t$ ,  $\sigma RT\Delta c_s$  changes with kinetics similar to that of the solution change. Thus, equation (A1) can be written as,

$$J_v(t) = L_p(\Delta p^\infty - \sigma RT\Delta c_s^\infty) \left(1 - e^{-t/\tau_p}\right) \quad (B1)$$

where  $\Delta c_s^\infty$  is the presumed asymptotic value of  $\Delta c_s$  as  $t$  approaches infinity. For small  $t = t_\epsilon$ , this equation can be approximated with,

$$J_v(t_\epsilon) = L_p(\Delta p^\infty - \sigma RT\Delta c_s^\infty) (t_\epsilon/\tau_p) \quad (B2)$$

Furthermore, since the volume change can be approximated with a single-exponential curve, we will have,

$$J_v(t_\epsilon) = [(V_\infty - V_0)/\tau_v] (1 - t_\epsilon/\tau_v) \quad (B3)$$

Combining equations (B2) and (B3), we will have the hydraulic conductivity as,

$$L_p = [(V_\infty - V_0)/(\Delta p^\infty - \sigma RT\Delta c_s^\infty)] (\tau_p/\tau_v) (1/t_\epsilon - 1/\tau_v) \quad (B4)$$

Thus, from (B4) we can calculate the osmotic permeability coefficient,

$$P_f = RTL_p/V_w A \quad (B5)$$

Note that (a) the relationship between  $L_p$  (and thus,  $P_f$ ) and  $\tau_v$  in the equation (B4) is not a simple inverse relationship as was the case in equations (3) and (4) (in Methods); and, (b) ignoring the contribution of  $\sigma RT\Delta c_s^\infty$  in the equation (B4) would lead to underestimating  $L_p$  and  $P_f$ . For estimates of  $P_f$  based on volume decrease measurements (e.g., in Group 1),  $\sigma RT\Delta c_s^\infty$  is rather small; therefore, the underestimation error is also small. However, for the estimates based on volume increase measurements, ignoring  $\sigma RT\Delta c_s^\infty$  has produced  $P_f$  estimates that are significantly smaller than the actual  $P_f$  (see Table 1).

#### References

- Belyantseva, I.A., Frolenkov, G.I., Wade, J.B., Mammano, F., Kachar, B., 2000. Water permeability of cochlear outer hair cells: characterization and relationship to electromotility. *J. Neurosci.* 20, 8996–9003.
- Bentley, P.J., 2002. Endocrines and Osmoregulation: A Comparative Account in Vertebrates, second ed. Springer, New York.

- Bernard, C., Ferrary, E., Sterkers, O., 1986. Production of endolymph in the semi-circular canal of the frog *Rana esculenta*. *J. Physiol.* 371, 17–28.
- Carey, M.B., Zelick, R., 1993. The effect of sound level, temperature and dehydration on the brainstem auditory evoked potential in anuran amphibians. *Hear. Res.* 70, 216–228.
- Chertoff, M.E., Brownell, W.E., 1994. Characterization of cochlear outer hair cell turgor. *Am. J. Phys.* 266, C467–C479.
- Dulon, D., Schacht, J., 1992. Motility of cochlear outer hair cells. *Am. J. Otol.* 13, 108–112.
- Echevarria, M., Verkman, A.S., 1992. Optical measurement of osmotic water transport in cultured cells. Role of glucose transporters. *J. Gen. Physiol.* 99, 573–589.
- Farahbakhsh, N.A., Narins, P.M., 2006. Slow motility in hair cells of the frog amphibian papilla:  $Ca^{2+}$ -dependent shape changes. *Hear. Res.* 212, 140–159.
- Farahbakhsh, N.A., Narins, P.M., 2008. Slow motility in hair cells of the frog amphibian papilla: myosin light chain-mediated shape change. *Hear. Res.* 241, 7–17.
- Farahbakhsh, N.A., Zelaya, J.E., Narins, P.M., 2010. Osmotic properties of auditory hair cells in the leopard frog: evidence for water-permeable channels. *ARO Abstracts* 33, 29.
- Farmer, R.E., Macey, R.I., 1970. Perturbation of red cell volume: rectification of osmotic flow. *Biochim. Biophys. Acta.* 196, 53–65.
- Grosse, T., Heid, I., Simaels, J., Beck, F., Nagel, W., Van Driessche, W., Dorge, A., 2001. Changes in element composition of A6 cells following hypotonic stress. *Pflügers. Arch.* 442, 297–303.
- Hillman, S.S., 1980. Physiological correlates of differential dehydration tolerance in anuran amphibians. *Copeia*, 125–129.
- Hoffmann, E.K., Lambert, I.H., Pedersen, S.F., 2009. Physiology of cell volume regulation in vertebrates. *Physiol. Rev.* 89, 193–277.
- Ishibashi, K., Hara, S., Kondo, S., 2009. Aquaporin water channels in mammals. *Clin. Exp. Nephrol.* 13, 107–117.
- Kedem, O., Katchalsky, A., 1958. Thermodynamic analysis of the permeability of biological membranes to non-electrolytes. *Biochim. Biophys. Acta.* 27, 229–246.
- Lakowicz, J.R., 1983. Principles of Fluorescence Spectroscopy. Plenum Press, New York.
- Lohr, J.W., 1990. Isovolumetric regulation of renal proximal tubules in hypotonic medium. *Ren. Physiol. Biochem.* 13, 233–240.
- Lohr, J.W., Grantham, J.J., 1986. Isovolumetric regulation of isolated S2 proximal tubules in anisotonic media. *J. Clin. Invest.* 78, 1165–1172.
- Lohr, J.W., Yohe, L., 2000. Isovolumetric regulation of rat glial cells during development and correction of hypo-osmolality. *Neurosci. Lett.* 286, 5–8.
- Manley, G.A., 2000. Cochlear mechanisms from a phylogenetic viewpoint. *Proc. Natl. Acad. Sci. U S A* 97, 11736–11743.
- Miller, M., Nasiri, A., Farahbakhsh, N.A., Simmons, D.D., Narins, P.M., 2010. Identification of Aquaporin-4 in *Rana pipiens* AP hair cells. *ARO Abstracts* 33, 217.
- Nishimoto, G., Sasaki, G., Yaoita, E., Nameta, M., Li, H., Furuse, K., Fujinaka, H., Yoshida, Y., Mitsudome, A., Yamamoto, T., 2007. Molecular characterization of water-selective AQP (EbAQP4) in hagfish: insight into ancestral origin of AQP4. *Am. J. Physiol. Regul. Integr. Comp. Physiol.* 292, R644–R651.
- Probstein, G.P., 1994. Physicochemical Hydrodynamics: an Introduction. J Wiley, New York.
- Quesada, O., Franco, R., Hernandez-Fonseca, K., Tuz, K., 2000. Isovolumic regulation in nervous tissue: a novel mechanism of cell volume regulation. *Adv. Exp. Med. Biol.* 483, 219–225.
- Ratnanather, J.T., Zhi, M., Brownell, W.E., Popel, A.S., 1996. Measurements and a model of the outer hair cell hydraulic conductivity. *Hear. Res.* 96, 33–40.
- Souza, M.M., Boyle, R.T., Lieberman, M., 2000. Different physiological mechanisms control isovolumetric regulation and regulatory volume decrease in chick embryo cardiomyocytes. *Cell. Biol. Int.* 24, 713–721.
- Suzuki, M., Tanaka, S., 2009. Molecular and cellular regulation of water homeostasis in anuran amphibians by aquaporins. *Comp. Biochem. Physiol. A Mol. Integr. Physiol.* 153, 231–241.
- Van Driessche, W., De Smet, P., Li, J., Allen, S., Zizi, M., Mountian, I., 1997. Isovolumetric regulation in a distal nephron cell line (A6). *Am. J. Phys.* 272, C1890–C1898.
- Verkman, A.S., 1989. Mechanisms and regulation of water permeability in renal epithelia. *Am. J. Phys.* 257, C837–C850.
- Yang, B., Verkman, A.S., 1997. Water and glycerol permeabilities of aquaporins 1–5 and MIP determined quantitatively by expression of epitope-tagged constructs in *Xenopus* oocytes. *J. Biol. Chem.* 272, 16140–16146.
- Zhi, M., Ratnanather, J.T., Ceyhan, E., Popel, A.S., Brownell, W.E., 2007. Hypotonic swelling of salicylate-treated cochlear outer hair cells. *Hear. Res.* 228, 95–104.